

A FULLY COUPLED MODEL IN CARDIAC ELECTROMECHANICS AND ITS EFFICIENT NUMERICAL APPROXIMATION

OLAF DÖSSEL, TOBIAS GERACH, EKATERINA KOVACHEVA, LAURA LINDNER,
AXEL LOEWE, JONATHAN FRÖHLICH AND CHRISTIAN WIENERS¹

Abstract. We develop an efficient numerical realization of the monodomain model which describes the basic electrophysiology in the human heart, coupled with cardiac electromechanics. Here we give a comprehensive definition of all model components and the resulting coupled PDE and ODE system and we summarize a full parameter set for realistic simulations. Numerical results for the coupled model are presented and a detailed convergence study for the monodomain equation demonstrate the approximation properties of our approach.

1991 Mathematics Subject Classification. 65N30.

July 23, 2020.

1. INTRODUCTION

Depolarization waves in the heart are the fundamental electrophysiological phenomenon governing cardiac function and are described by the basic model for the cardiac reaction-diffusion system: the bidomain equations for electrical potentials across the cell membrane governing the spread of the depolarization waves. The cardiac electrophysiological system triggers mechanical contractions of the heart muscle, which is modeled as a time-varying elastic body. The electrical cellular transmembrane voltages are given as solutions to nonlinear reaction-diffusion equations on a manifold. This PDE system is coupled with an ODE system to determine the transmembrane currents.

The full model approximates the electric potential, the concentration of various ions, several gating variables, the deformation of the cardiac tissue, and further variables for the coupling to the circulatory system. For the individual systems, thorough benchmarks have been conducted, see e.g. [Niederer et al., 2011] or [Land et al., 2015]. Our purpose is to construct a system of differential equations and to collect a full parameter set, which is able to describe all relevant mechanisms qualitatively and quantitatively correctly.

For the fully coupled model we present a discretization scheme based on a second order splitting of PDE and ODE components and including asymptotically exact integrators for the very fast evolution of the gating variables. For the monodomain subsystem, the convergence properties of the discretization scheme are studied in detail, which shows that the overall model is efficient and accurate.

Remark. This document collects preliminary results of the PhD projects of L. Linder and J. Fröhlich, and it will be a basis for a joint publication with our partners in near future.

Keywords and phrases: cardiac modeling and simulation, electrophysiology, monodomain equation, electromechanics

¹ Karlsruhe Institute of Technology (KIT), Germany. Email: christian.wieners@kit.edu

CONTENTS

1. Introduction	1
2. A fully coupled model in cardiac electrophysiology	3
3. The monodomain equation	4
4. A splitting method for the monodomain equation	5
5. The ten Tusscher cell model	7
6. The Courtemanche cell model	12
7. A model for cardiac electromechanics	16
8. The cell-contraction model	20
9. The circulatory system	22
Appendix A. Monodomain parameters	24
Appendix B. Hyperelastic parameters	28
Appendix C. Circulatory System Parameters	29
Acknowledgments	29
References	29

2. A FULLY COUPLED MODEL IN CARDIAC ELECTROPHYSIOLOGY

A mathematical model for depolarization waves and the contraction of the heart comprises a time-dependent nonlinear PDE system for the electric potential and the mechanical deformation, coupled with ODEs for ion concentrations and gating variables, several ODEs for the blood pressure in the cardiac chambers, and a surrogate model for the interaction with the circulatory system. Our fully-coupled model describes the following mechanisms:

- To initiate a heartbeat, an electric impulse is initiated in the sinus node cells. From there, the depolarization wave is captured by and propagates through the cardiac tissue.
- Intracellular and extracellular electrical potentials, which influence the opening and closing of transmembrane ion channels and govern the concentration of ions in the cells.
- The increased calcium concentration activates the contraction of myofibrils in the cells, which results in a contraction of the heart muscle.
- The contraction of the heart muscle increases the pressure in the chambers, which results in the blood flow.

For a qualitatively correct and sufficiently accurate computational model, we numerically realize the following coupled electromechanical system, determined by

- a reference domain $\Omega \subset \mathbb{R}^3$ consisting of subdomains Ω_V for the ventricles, Ω_A for the atria, and Ω_T for surrounding tissue;
- the electric potential $V_m \in C^1([0, T], L_2(\Omega) \cap C^0([0, T], H^1(\Omega_V \cup \Omega_A)))$;
- a vector of ion concentrations and gating variables $w \in C^1([0, T], L_q(\Omega_V \cup \Omega_A; \mathbb{R}^N))$;
- the deformation vector $\varphi \in C^2([0, T], L_2(\Omega; \mathbb{R}^3)) \cap C^0([0, T], W^{1,p}(\Omega; \mathbb{R}^3))$;
- the stretch along the fibre and a vector of state variables describing the force development $(\gamma_f, g) \in C^1([0, T], L_q(\Omega_V \cup \Omega_A; \mathbb{R}^{1+K}))$;
- the blood pressure in the cardiac chambers $p \in C^1([0, T], \mathbb{R}^4)$;
- a vector of variables $z \in C^1([0, T], \mathbb{R}^M)$ modeling the circulatory system

and solving the coupled PDE – ODE system

$$\beta C_m \partial_t^\varphi V_m = \nabla^\varphi \cdot \sigma(\mathbf{f}^\varphi) \nabla^\varphi V_m - \beta I_{\text{ion}}(V_m, w, \gamma_f) + I_{\text{ext}}, \quad (1a)$$

$$\partial_t^\varphi w = G_w(w, V_m, \gamma_f), \quad (1b)$$

$$\rho \partial_t^2 \varphi = \text{div } \mathbf{P}(\mathbf{D}\varphi, \mathbf{f}^\varphi, \gamma_f), \quad (1c)$$

$$\partial_t^\varphi \gamma_f = G_{\gamma_f}(\gamma_f, \mathbf{D}\varphi, \mathbf{f}^\varphi, g, w), \quad (1d)$$

$$\partial_t^\varphi g = G_g(g, \gamma_f, \mathbf{D}\varphi, w), \quad (1e)$$

$$\partial_t p = G_p(p, z), \quad (1f)$$

$$\partial_t z = G_z(z, p), \quad (1g)$$

$$0 = G_C(z, |\Omega_{VL}^\varphi|, |\Omega_{VR}^\varphi|, |\Omega_{AL}^\varphi|, |\Omega_{AR}^\varphi|) \quad (1h)$$

with total derivative in time $\partial_t^\varphi w = \partial_t w + \nabla^\varphi \cdot (w \partial_t \varphi)$ and the covariant gradient ∇^φ , and where

- the equations (1a) and (1b) couples the parabolic equation of the potential with the ODE system describing the cell model which determined by (I_{ion}, G_w) , where the ion density (I_{ion}) and the gating mechanism G_w are specified in the next sections for the different models;
- the depolarization wave is initiated by an external impulse I_{ext} located at predefined nodes or natural cellular pacemakers with (I_{ion}, G_w) not exhibiting a stable resting state;
- the electric potential is determined by the monodomain equation and the electric conductivity $\sigma(\mathbf{f}^\varphi)$ depending on the fiber direction \mathbf{f}^φ in the deformed configuration;
- the deformation is activated by a strain $\mathbf{F}_a(\mathbf{f}^\varphi, \gamma_f)$ or a stress $\mathbf{P}_a(\mathbf{f}^\varphi, \gamma_f)$ along the fiber direction \mathbf{f}^φ , i.e., $\mathbf{P} = DW(\mathbf{D}\varphi \mathbf{F}_a(\mathbf{f}^\varphi, \gamma_f)^{-1})$ or $\mathbf{P} = DW(\mathbf{D}\varphi) + \mathbf{P}_a(\mathbf{f}^\varphi, g)$. The tension development is modeled by

a system of ODEs determined by (G_{γ_f}, G_g) depending on the deformation gradient $D\varphi$ and the vector of ion concentrations and gating variables w ;

- the interaction with the circulatory system is determined by the evolution (1f) of the pressure p described by G_p depending on the parameters z of the circulatory system subject to the constraint (1g) that the volume in the chambers $|\Omega_{VL}^\varphi|, |\Omega_{VR}^\varphi|, |\Omega_{AL}^\varphi|, |\Omega_{AR}^\varphi|$ evaluated from the deformation and the circulatory system coincide;
- in this model where the blood flow is not evaluated explicitly, we assume that the pressure is spatially constant in every chamber so the circulatory system couples to the deformation by $\mathbf{Pn} = p\mathbf{n}$ on the inner boundary;
- we assume $\mathbf{n} \cdot [\varphi] = 0$ along the pericardium.

The equations are complemented by initial values and boundary conditions.

The basic mathematical aspects of this electromechanical system are well understood as recently reviewed [Cherry et al., 2017, Franzone et al., 2014, Quarteroni et al., 2017]. First results on the analysis of stability and existence of the solution for the linearized electromechanical system are given in [Andreianov et al., 2015]. The extension to nonlinear elastic models is more involved; a nonlinear analysis of a very specific model for cardiac electromechanical activity is considered in [Pathmanathan et al., 2013]. A detailed numerical investigation of bioelectrical effects of mechano-electrical feedback is included in [Colli Franzone et al., 2017]. More specific considerations on fast parallel solvers for the solution of the discretized coupled system based on domain decomposition and multigrid techniques are considered in [Augustin et al., 2016, Franzone et al., 2015, Pavarino et al., 2017, Santiago et al., 2018].

3. THE MONODOMAIN EQUATION

In the first step, we only consider the monodomain model in the reference domain without deformation, which describes the electrophysiology independently in the ventricles and atria.

Therefore, let $\Omega_M = \Omega_V$ or $\Omega_M = \Omega_A$ be the domain and let (I_{ion}, G_w) the corresponding cell model in the ventricles and atria, respectively. The cell model is described by the transmembrane current density I_{ion} and the evolution of ion concentrations and gating variable determined by G_w . The ten Tusscher cell model for the ventricles is described in Sect. 5, and the Courtemanche cell model in Sect. 6.

In this section we only consider the electrophysiology on the fixed reference geometry, i.e., we have $\varphi = \text{id}$ and $\gamma_f = 0$.

The monodomain data. Depending on the fiber direction in the reference domain

$$\mathbf{f}: \Omega_M \longrightarrow S^2,$$

the conductivity tensor is given by

$$\boldsymbol{\sigma}(\mathbf{f}) = \sigma_l \mathbf{f} \otimes \mathbf{f} + \sigma_t (\mathbf{I} - \mathbf{f} \otimes \mathbf{f}) \in \mathbb{R}_{\text{sym}}^{3 \times 3}$$

with conductivity parameters $\sigma_l \geq 0$ in longitudinal and $\sigma_t \geq 0$ in transversal direction.

In our model we use a prescribed pacing mechanism, the depolarization waves are initiated by an external stimulus $I_{\text{ext}} \in L_2((0, T); L_2(\Omega))$ modeling the activation of the electric potential at the Purkinje Muscle Junctions in the ventricles and the sinus node in the atria. Here we define

$$I_{\text{ext}}(t, x) = \begin{cases} A_j & t \in (t_j, t_j + \tau_j), \ x \in \mathcal{N}_{\text{ext}}^h \\ 0 & \text{else} \end{cases} \quad (2)$$

at a subset of the finite element nodal points $\mathcal{N}_{\text{ext}}^h \subset \mathcal{N}^h \subset \overline{\Omega}_M$, depending on the starting time $t_j \geq 0$, duration $\tau_j > 0$, and amplitude $A_j > 0$. The values at the nodal points $z \in \mathcal{N}^h$ are interpolated by the nodal basis functions ϕ_z , which defines $I_{\text{ext}} \in L_2(0, T; \Omega_M)$ by $I_{\text{ext}}(t, x) = \sum_{z \in \mathcal{N}_h} I_{\text{ext}}(t, z) \phi_z(x)$. Nevertheless, in the

approximation only the values at the nodal points are used in the numerical scheme, cf. Fig. 1.

A second possibility to define the external stimulus is the use of a sigmoid function instead of the step function defined above. Therefor we use the values A_j , t_j , τ_j and additionally a scaling factor for the steepness of the sigmoid function denoted by s_j . Then we define

$$I_{\text{ext}}(t, x) = \frac{A_j}{2} \left((1 + \tanh(s_j(t - t_j))) - (1 + \tanh(s_j(t - (t_j + \tau_j)))) \right) \quad (3)$$

for all nodal points $x \in \mathcal{N}^h$. For all nodal points $x \notin \mathcal{N}_{\text{ext}}^h$ we set $A_j = 0$ such that $I_{\text{ext}}(t, x) = 0 \forall t$.

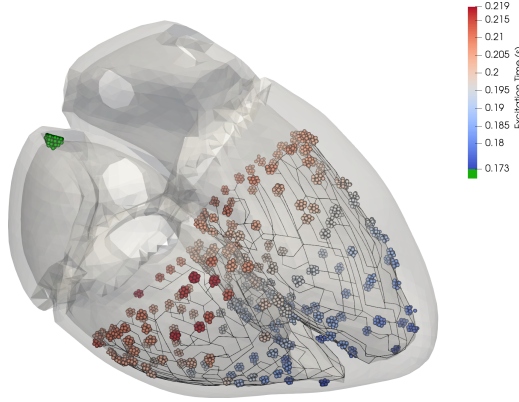


FIGURE 1. Illustration of the Purkinje fibers and the stimulus points at the end of each branch are shown with their respective activation time. The external stimulus points of the sinus node at $t = 0$ s is shown in green.

The monodomain evolution. We consider the coupled diffusion-reaction equation in $(0, T) \times \Omega_M$ for the electric potential V_m and the vector of gating variables w

$$\beta C_m \partial_t V_m = \nabla \cdot \sigma \nabla V_m - \beta I_{\text{ion}}(V_m, w) + I_{\text{ext}}, \quad (4a)$$

$$\partial_t w = G_w(w, V_m, \gamma_f) \quad (4b)$$

subject to the initial values at $t = 0$ in Ω_M

$$V_m(0) = V_m^0, \quad (4c)$$

$$w(0) = w^0, \quad (4d)$$

and homogeneous Neumann boundary conditions on $(0, T) \times \partial\Omega$

$$\mathbf{n} \cdot \sigma \nabla V_m = 0. \quad (4e)$$

4. A SPLITTING METHOD FOR THE MONODOMAIN EQUATION

The idea of the splitting methods for the coupled model (4a) and (4b) is a decoupling into a parabolic problem without reaction term

$$\beta C_m \partial_t V_m = \nabla \cdot \sigma \nabla V_m$$

and independent ODEs for $x \in \Omega$ without the diffusion term

$$\begin{aligned} C_m \partial_t V_m &= -I_{\text{ion}}(V_m, w) + I_{\text{ext}}, \\ \partial_t w &= G_w(w, V_m). \end{aligned}$$

Let $\mathbf{V}^h \subset H^1(\Omega)$ be a conforming finite element space corresponding to a tetrahedral mesh $\Omega_M^h = \bigcup_{K \in \mathcal{K}_h} K$, and let $\mathcal{N}^h \subset \overline{\Omega}_M$ be associated nodal points. Here, we use linear elements in the tetrahedron K with linear nodal basis functions ϕ_x , where $x \in \mathcal{N}_h$ are the corner points.

Both, the electric potential V_m and the gating variables are approximated in the finite element space \mathbf{V}^h and thus represented by the nodal values.

Let $N \in \mathbb{N}$ be the number of time steps, and set $t_n = n\Delta t$ with time steps size $\Delta t = T/N$. Furthermore, let $M \in \mathbb{N}$ be the number of substeps for the approximation of the cell models. Then, starting with initial values $V_m^{h,0} = V_m^0$ and $w^{h,0} = w_0$, the symmetric Strang splitting with substepping is defined for $n = 1, 2, \dots, N$ as follows:

- (1) Independently for every nodal point $x \in \mathcal{N}^h$, compute in $(t_{n-1}, t_{n-1/2})$ an approximation of the ODE

$$\begin{aligned} C_m \partial_t V_m^h &= -I_{\text{ion}}(V_m^h, w^h) + I_{\text{ext}}, \\ \partial_t w^h &= G_w(w^h, V_m^h) \end{aligned}$$

with initial values $V_m^h(t_{n-1}) = V_m^{h,n-1}$ and $w^h(t_{n-1}) = w^{h,n-1}$ using M time steps of step size $\frac{\Delta t}{2M}$; then, set $V_m^{h,n-1/2} = V_m^h(t_{n-1/2})$ and $w^{h,n-1/2} = w^h(t_{n-1/2})$.

- (2) For given $V_m^{h,n-1/2} \in \mathbf{V}^h$, compute $\hat{V}_m^{h,n-1/2} \in \mathbf{V}^h$ with the implicit Euler method, i.e., solve

$$\int_{\Omega_M} \left(\hat{V}_m^{h,n-1/2} \phi^h + \frac{\Delta t}{\beta C_m} \nabla \hat{V}_m^{h,n-1/2} \cdot \boldsymbol{\sigma} \nabla \phi^h \right) dx = \int_{\Omega_M} V_m^{h,n-1/2} \phi^h dx, \quad \phi^h \in \mathbf{V}^h.$$

- (3) Repeat the first step in $(t_{n-1/2}, t_n)$ starting with $(\hat{V}_m^{h,n-1/2}, w^{h,n-1/2})$; this gives $(V_m^{h,n}, w^{h,n})$.

Time integration for the ODE system. To solve the ODE system

$$\begin{aligned} C_m \partial_t V_m^h &= -I_{\text{ion}}(V_m^h, w^h) + I_{\text{ext}}, \\ \partial_t w^h &= G_w(w^h, V_m^h) \end{aligned}$$

with initial values $V_m^h(t_{n-1}) = V_m^{h,n-1}$ and $w^h(t_{n-1}) = w^{h,n-1}$ independently in every nodal point $x \in \mathcal{N}^h$ in (t_{n-1}, t_n) we tested different time integration methods. The scheme for the second equation stays always the same and is described in the sections where the different cell models are explained. For the first equation we implemented the simple explicit Euler method and the two step Adams Bashforth method. For the explicit Euler method we have

$$V_m^{h,n} = V_m^{h,n-1} - \frac{\Delta t}{C_m} (I_{\text{ion}}(V_m^{h,n-1}, w^{h,n-1}) - I_{\text{ext}}).$$

For the twostep Adams Bashforth method we compute the first two solutions with the explicit Euler method as given in this section and for every further timestep we use the following:

$$V_m^{h,n} = V_m^{h,n-1} - \frac{\Delta t}{2C_m} \left(3(I_{\text{ion}}(V_m^{h,n-1}, w^{h,n-1}) - I_{\text{ext}}) - (I_{\text{ion}}(V_m^{h,n-2}, w^{h,n-2}) - I_{\text{ext}}) \right).$$

Numerical results on the mesh in Fig. 2 are presented in Fig. 3.

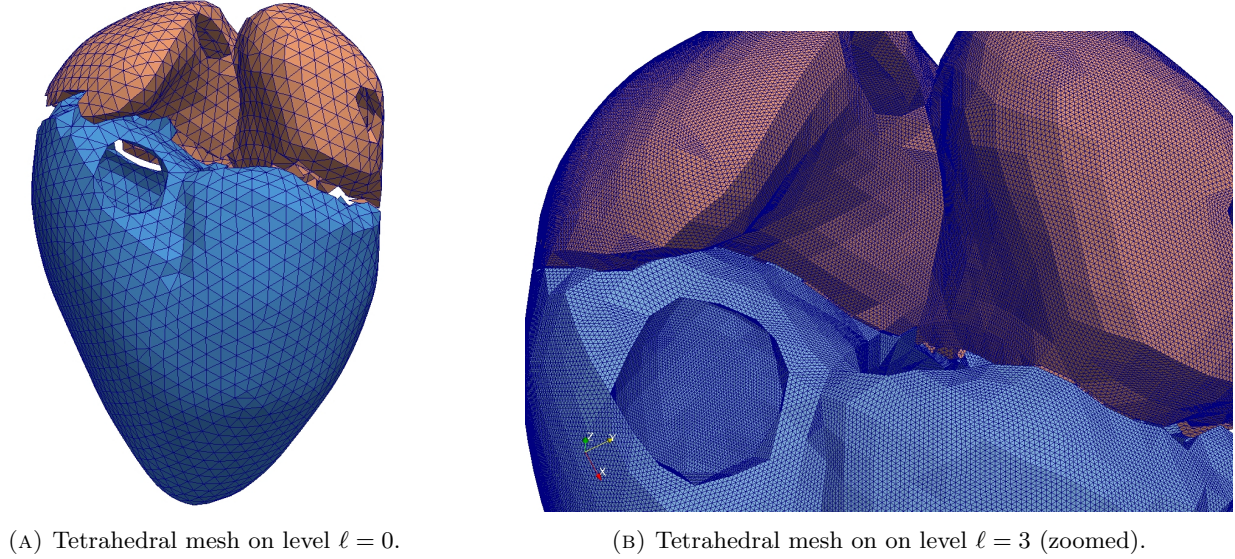


FIGURE 2. Reference geometry approximating ventricles and atria on level $\ell = 0$ and with three uniform refinement steps.

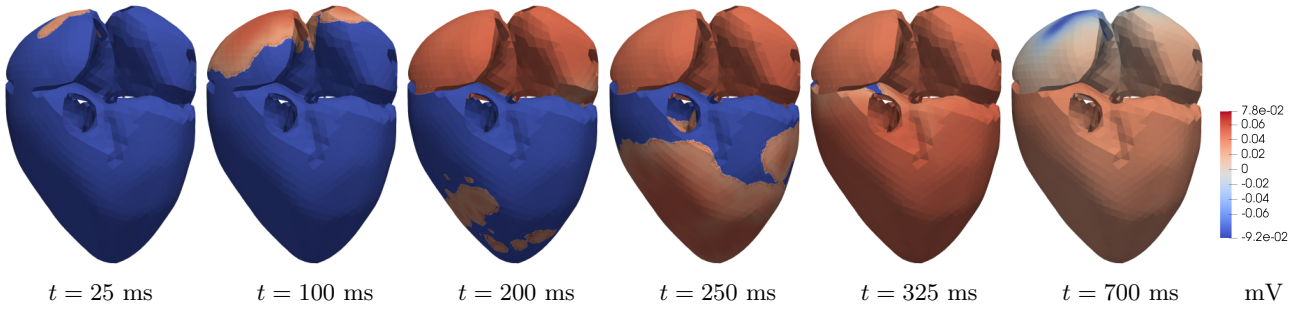


FIGURE 3. Evolution of a depolarization wave on the ventricles and atria: In this model, the wave is initiated via external stimuli starting at the sinus node located in the wall of the right atrium of the heart and then propagates by electrophysiologic mechanisms. The electric potential is computed with conforming finite elements, which are coupled with an abstract interface to the ODE system describing the electrophysiology of the cell membranes at every nodal point. The time stepping is realized by a splitting scheme. The system is computed in parallel and requires approximately 8.5 million tetrahedra to faithfully represent a physiologically accurate propagation of the cardiac depolarization wave.

5. THE TEN TUSSCHER CELL MODEL

In the ventricles, we use the ten Tusscher cell model [ten Tusscher and Panfilov, 2006]. The model is extended by a stretch-activated channel based on the formulation in [Kohl et al., 2001, Tavi et al., 1998].

Here, the model involves the ion concentration of calcium Ca , Ca_{SS} , Ca_{SR} , sodium Na , and potassium K , and 13 gating variables

$$w = (\text{Ca}, \text{Ca}_{\text{SS}}, \text{Ca}_{\text{SR}}, \text{Na}, \text{K}, \bar{R}, \bar{O}, m, h, j, x_{r1}, x_{r2}, x_s, s, r, d, f, f_2, f_{\text{Ca}})$$

and depending on the constants $R, T, F, z, \text{Na}_e, \text{K}_e, \text{Ca}_e, G_{\text{Na}}, G_{\text{CaL}}, G_{\text{Ks}}, G_{\text{to}}, G_{\text{Kr}}, G_{\text{K1}}, G_{\text{pCa}}, G_{\text{pK}}, G_{\text{bNa}}, G_{\text{SAC}}, p_{\text{KNa}}, V_{\text{m,CaL}}, V_{\text{m,pK},1}, V_{\text{m,pK},1}, k_{\text{NaCa}}, \gamma, \alpha, K_{\text{mNa}i}, K_{\text{mCa}}, k_{\text{sat}}, P_{\text{NaK}}, K_{\text{mK}}, K_{\text{mNa}}, K_{\text{pCa}}, E_{\text{SAC}}, \kappa_e$ and α_{SAC} for ionic currents and the constants $V_c, V_{\text{SR}}, V_{\text{SS}}, V_{\text{leak}}, V_{\text{maxup}}, K_{\text{up}}, V_{\text{rel}}, V_{\text{xfer}}, k_1, k_2, k_3, k_4$, for the evolution of ion concentration all specified in Tab. 2.

In the equation for the potential $C_m \partial_t V_m = I_{\text{ion}}(V_m, w, \gamma_f) + I_{\text{ext}}$, the transmembrane current density I_{ion} is given by

$$\begin{aligned} I_{\text{ion}}(V_m, w, \gamma_f) = & I_{\text{Na}}(V_m, \text{Na}, m, h, j) + I_{\text{CaL}}(V_m, d, f, f_2, f_{\text{Ca}}, \text{Ca}_{\text{SS}}) + I_{\text{Ks}}(V_m, \text{K}, \text{Na}, x_s) + I_{\text{to}}(V_m, \text{K}, r, s) \\ & + I_{\text{Kr}}(V_m, \text{K}, x_{r1}, x_{r2}) + I_{\text{K1}}(V_m, \text{K}) + I_{\text{NaCa}}(V_m, \text{Na}, \text{Ca}) + I_{\text{NaK}}(V_m, \text{Na}) + I_{\text{pCa}}(\text{Ca}) \\ & + I_{\text{pK}}(V_m, \text{K}) + I_{\text{bCa}}(V_m, \text{Ca}) + I_{\text{bNa}}(V_m, \text{Na}) + I_{\text{SAC}}(V_m, \gamma_f) \end{aligned}$$

combines the contribution of different ions, where

$$\begin{aligned} I_{\text{Na}}(V_m, \text{Na}, m, h, j) &= G_{\text{Na}} m^3 h j (V_m - E_{\text{Na}}(\text{Na})), \\ I_{\text{CaL}}(V_m, d, f, f_2, f_{\text{Ca}}, \text{Ca}_{\text{SS}}) &= 4 \frac{(V_m - V_{\text{m,CaL}}) F^2}{RT} \frac{0.25 \text{Ca}_{\text{SS}} \exp(2(V_m - V_{\text{m,CaL}}) \frac{F}{RT}) - \text{Ca}_e}{\exp(2(V_m - V_{\text{m,CaL}}) \frac{F}{RT}) - 1} G_{\text{CaL}} f f_2 f_{\text{Ca}} d, \\ I_{\text{Ks}}(V_m, \text{K}, \text{Na}, x_s) &= G_{\text{Ks}} x_s^2 (V_m - E_{\text{Ks}}(\text{K}, \text{Na})), \\ I_{\text{to}}(V_m, \text{K}, r, s) &= G_{\text{to}} r s (V_m - E_{\text{K}}(\text{K})), \\ I_{\text{Kr}}(V_m, \text{K}, x_{r1}, x_{r2}) &= G_{\text{Kr}} \sqrt{\frac{K_e}{5.4}} x_{r1} x_{r2} (V_m - E_{\text{K}}(\text{K})), \\ I_{\text{K1}}(V_m, \text{K}) &= G_{\text{K1}} \sqrt{\frac{K_e}{5.4}} x_{\text{K1},\infty}(V_m, \text{K}) (V_m - E_{\text{K}}(\text{K})), \\ I_{\text{NaCa}}(V_m, \text{Na}, \text{Ca}) &= k_{\text{NaCa}} \frac{\exp(\gamma V_m \frac{F}{RT}) \text{Na}^3 \text{Ca}_e - \exp((\gamma - 1) V_m \frac{F}{RT}) \text{Na}_e^3 \text{Ca} \alpha}{(K_{\text{mNa}i}^3 + \text{Na}_e^3)(K_{\text{mCa}} + \text{Ca}_e)(1 + k_{\text{sat}} \exp((\gamma - 1) V_m \frac{F}{RT}))}, \\ I_{\text{NaK}}(V_m, \text{Na}) &= P_{\text{NaK}} \frac{K_e \text{Na}}{(\text{K}_e + K_{\text{mK}})(\text{Na} + K_{\text{mNa}})(1 + 0.1245 \exp(-0.1 V_m \frac{F}{RT}) + 0.0353 \exp(-V_m \frac{F}{RT}))}, \\ I_{\text{pCa}}(\text{Ca}) &= G_{\text{pCa}} \frac{\text{Ca}}{K_{\text{pCa}} + \text{Ca}}, \\ I_{\text{pK}}(V_m, \text{K}) &= G_{\text{pK}} \frac{V_m - E_{\text{K}}(\text{K})}{1 + \exp((V_{\text{m,pK},1} - V_m)/V_{\text{m,pK},2})}, \\ I_{\text{bCa}}(V_m, \text{Ca}) &= G_{\text{bCa}} (V_m - E_{\text{Ca}}(\text{Ca})), \\ I_{\text{bNa}}(V_m, \text{Na}) &= G_{\text{bNa}} (V_m - E_{\text{Na}}(\text{Na})), \\ I_{\text{SAC}}(V_m, \gamma_f) &= G_{\text{SAC}} \frac{V_m - E_{\text{SAC}}}{1 + \kappa_e \exp(-\alpha_{\text{SAC}} \gamma_f)} \end{aligned}$$

with the reverse potentials

$$\begin{aligned} E_{\text{Ca}}(\text{Ca}) &= \frac{RT}{zF} \log \frac{\text{Ca}_e}{\text{Ca}} , \\ E_{\text{Na}}(\text{Na}) &= \frac{RT}{zF} \log \frac{\text{Na}_e}{\text{Na}} , \\ E_{\text{K}}(\text{K}) &= \frac{RT}{zF} \log \frac{\text{K}_e}{\text{K}} , \\ E_{\text{Ks}}(\text{K}, \text{Na}) &= \frac{RT}{F} \log \frac{\text{K}_e + p_{\text{KNa}} \text{Na}_e}{\text{K} + p_{\text{KNa}} \text{Na}} , \end{aligned}$$

and

$$\begin{aligned} \alpha_{\text{K1}}(V_m, \text{K}) &= \frac{0.1}{1 + \exp(0.06(-200 + V_m - E_{\text{K}}(\text{K})))} , \\ \beta_{\text{K1}}(V_m, \text{K}) &= \frac{3 \exp(0.0002(100 + V_m - E_{\text{K}}(\text{K}))) + \exp(0.1(-10 + V_m - E_{\text{K}}(\text{K})))}{1 + \exp(-0.5(V_m - E_{\text{K}}(\text{K})))} , \\ x_{\text{K1},\infty}(V_m, \text{K}) &= \frac{\alpha_{\text{K1}}(V_m, \text{K})}{\alpha_{\text{K1}}(V_m, \text{K}) + \beta_{\text{K1}}(V_m, \text{K})} . \end{aligned}$$

For the evolution of ion concentrations and gating variables (4b) we specify every component of w independently.

The evolution of ion concentrations. We have

$$\begin{aligned} \partial_t \text{Na} &= -\frac{1}{V_c F} \left(I_{\text{Na}}(V_m, \text{Na}, m, h, j) + I_{\text{bNa}}(V_m, \text{Na}) + 3I_{\text{NaK}}(V_m, \text{Na}) + 3I_{\text{NaCa}}(V_m, \text{Na}, \text{Ca}) \right) , \\ \partial_t \text{K} &= -\frac{1}{V_c F} \left(I_{\text{K1}}(V_m, \text{K}) + I_{\text{NaCa}}(V_m, \text{Na}, \text{Ca}) + I_{\text{to}}(V_m, \text{K}, r, s) + I_{\text{Kr}}(V_m, \text{K}, x_{r1}, x_{r2}) \right. \\ &\quad \left. + I_{\text{Ks}}(V_m, \text{K}, \text{Na}, x_s) - 2I_{\text{NaK}}(V_m, \text{Na}) + I_{\text{pCa}}(\text{Ca}) + I_{\text{ext}} \right) , \\ \partial_t \text{Ca} &= -\frac{1}{2V_c F} \left(I_{\text{bCa}}(V_m, \text{Ca}) + I_{\text{pCa}}(\text{Ca}) - 2I_{\text{NaCa}}(V_m, \text{Na}, \text{Ca}) \right) \\ &\quad + \frac{V_{\text{SR}}}{V_c} \left(I_{\text{leak}}(\text{Ca}, \text{Ca}_{\text{SR}}) - I_{\text{up}}(\text{Ca}) + I_{\text{xfer}}(\text{Ca}, \text{Ca}_{\text{SS}}) \right) , \\ \partial_t \text{Ca}_{\text{SR}} &= I_{\text{up}}(\text{Ca}) - I_{\text{rel}}(\text{Ca}_{\text{SR}}, \text{Ca}_{\text{SS}}, \bar{R}) - I_{\text{leak}}(\text{Ca}, \text{Ca}_{\text{SR}}) , \\ \partial_t \text{Ca}_{\text{SS}} &= -\frac{1}{2V_{\text{SS}} F} I_{\text{CaL}}(V_m, d, f, f_2, f_{\text{Ca}}) + \frac{V_{\text{SR}}}{V_{\text{SS}}} I_{\text{rel}}(\text{Ca}_{\text{SR}}, \text{Ca}_{\text{SS}}, \bar{R}) - \frac{V_{\text{C}}}{V_{\text{SS}}} I_{\text{xfer}}(\text{Ca}, \text{Ca}_{\text{SS}}) \end{aligned}$$

with

$$\begin{aligned} I_{\text{leak}}(\text{Ca}, \text{Ca}_{\text{SR}}) &= V_{\text{leak}}(\text{Ca}_{\text{SR}} - \text{Ca}) , \\ I_{\text{up}}(\text{Ca}) &= \frac{V_{\text{maxup}}}{1 + K_{\text{up}}^2 / \text{Ca}^2} , \\ I_{\text{rel}}(\text{Ca}_{\text{SR}}, \text{Ca}_{\text{SS}}, \bar{R}) &= V_{\text{rel}} \bar{O}(\text{Ca}_{\text{SS}}, \bar{R}) (\text{Ca}_{\text{SR}} - \text{Ca}_{\text{SS}}) , \\ I_{\text{xfer}}(\text{Ca}, \text{Ca}_{\text{SS}}) &= V_{\text{xfer}} (\text{Ca}_{\text{SS}} - \text{Ca}) , \end{aligned}$$

where the proportion of open I_{rel} channels is given by

$$\bar{O}(\text{Ca}_{\text{SS}}, \bar{R}) = \frac{k_1 \text{Ca}_{\text{SS}}^2 \bar{R}}{k_3 + k_1 \text{Ca}_{\text{SS}}^2}$$

depending on the proportion of closed I_{rel} channels \bar{R} , which is modeled by a Hodgkin-Huxley type equation

$$\partial_t \bar{R} = \alpha_{\bar{R}}(1 - \bar{R}) - \beta_{\bar{R}}(\text{CaSS})\bar{R}$$

with

$$\alpha_{\bar{R}} = k_4, \quad \beta_{\bar{R}}(\text{CaSS}) = k_2 \text{CaSS}.$$

The gating mechanism. Gating variables y are described by a Hodgkin-Huxley type equation

$$\partial_t y = \alpha_y(V_m)(1 - y) - \beta_y(V_m)y, \quad (5)$$

where α_y and β_y are nonnegative functions of V_m , cf. [Cronin and Jane, 1987]. In case of constant coefficients α_y and β_y , we obtain the solution of the linear ODE

$$y(t) = \frac{\alpha_y}{\alpha_y + \beta_y} - \left(\frac{\alpha_y}{\alpha_y + \beta_y} - y(t_{n-1}) \right) \exp \left(-(\alpha_y + \beta_y)(t - t_{n-1}) \right), \quad t \in [t_{n-1}, t_n]. \quad (6)$$

This expression is used in the time-stepping scheme, i.e. y^n is computed from y^{n-1} with (6) by inserting $\alpha_y^{n-1} = \alpha_y(V_m^{n-1})$ and $\beta_y^{n-1} = \beta_y(V_m^{n-1})$.

Thus, we specify directly

$$\tau_y(V_m) = \frac{1}{\alpha_y(V_m) + \beta_y(V_m)}, \quad y_\infty(V_m) = \frac{\alpha_y(V_m)}{\alpha_y(V_m) + \beta_y(V_m)},$$

from which $\alpha_y(V_m)$ and $\beta_y(V_m)$ can be computed.

The gating evolution in the ten Tusscher model. In the following, all expressions depending on V_m are given in mV, i.e., in $\exp((35 + V_m)/5)$ the qualities 35 and 5 have the physical unit mV. The gating variables $y \in \{m, h, j, x_{r1}, x_{r2}, x_s, s, r, d, f, f_2\}$ are determined by

$$\tau_m(V_m) = \frac{1}{1 + \exp((-60 - V_m)/5)} \left(\frac{0.1}{1 + \exp((35 + V_m)/5)} + \frac{0.1}{1 + \exp((-50 + V_m)/200)} \right),$$

$$m_\infty(V_m) = \frac{1}{\left(1 + \exp((-56.86 - V_m)/9.03)\right)^2},$$

$$\tau_h(V_m) = \begin{cases} \frac{0.13(1 + \exp(-(V_m + 10.66)/11.1))}{0.77} & V_m \geq -40, \\ \left(0.057 \exp(-(V_m + 80)/6.8) + 2.7 \exp(0.079V_m) + 3.1 \cdot 10^5 \exp(0.3485V_m) \right)^{-1} & \text{else,} \end{cases}$$

$$h_\infty(V_m) = \frac{1}{\left(1 + \exp((71.55 + V_m)/7.43)\right)^2},$$

$$\tau_j(V_m) = \begin{cases} \frac{1 + \exp(-0.1(V_m + 32))}{0.6 \exp(0.057V_m)} & V_m \geq -40, \\ \left(\frac{(-2.5428 \cdot 10^4 \exp(0.24444V_m) - 6.948 \cdot 10^{-6} \exp(-0.04391V_m))(V_m + 37.78)}{1 + \exp(0.311(V_m + 79.23))} + \frac{0.02424 \exp(-0.01052V_m)}{1 + \exp(-0.1378(V_m + 40.14))} \right)^{-1} & \text{else,} \end{cases}$$

$$j_\infty(V_m) = h_\infty(V_m).$$

$$\begin{aligned}
\tau_d(V_m) &= \left(\frac{1.4}{1 + \exp((-35 - V_m)/13)} + 0.25 \right) \frac{1.4}{1 + \exp((5 + V_m)/5)} + \frac{1}{1 + \exp((50 - V_m)/20)}, \\
d_\infty(V_m) &= \frac{1}{1 + \exp((-8 - V_m)/7.5)}, \\
\tau_f(V_m) &= 1102.5 \exp\left(-\left(\frac{V_m + 27}{15}\right)^2\right) + \frac{200}{1 + \exp((13 - V_m)/10)} + \frac{180}{1 + \exp((30 + V_m)/10)} + 20, \\
f_\infty(V_m) &= \frac{1}{1 + \exp((20 + V_m)/7)}, \\
\tau_{f_2}(V_m) &= 600 \exp\left(-\frac{(V_m + 25)^2}{170}\right) + \frac{31}{1 + \exp((25 - V_m)/10)} + \frac{16}{1 + \exp((30 + V_m)/10)}, \\
f_{2,\infty}(V_m) &= \frac{0.67}{1 + \exp((35 + V_m)/7)} + 0.33, \\
\tau_{x_s}(V_m) &= \frac{1400}{\sqrt{1 + \exp((5 - V_m)/6)}} \frac{1}{1 + \exp((-35 + V_m)/15)} + 80, \\
x_{s,\infty}(V_m) &= \frac{1}{1 + \exp((-5 - V_m)/14)}, \\
\tau_r(V_m) &= 9.5 \exp\left(-\frac{(40 + V_m)^2}{1800}\right) + 0.8, \\
r_\infty(V_m) &= \frac{1}{1 + \exp((20 - V_m)/6)}, \\
\tau_s(V_m) &= 85 \exp\left(-\frac{(45 + V_m)^2}{320}\right) + \frac{5}{1 + \exp((-20 + V_m)/5)} + 3, \\
s_\infty(V_m) &= \frac{1}{1 + \exp((20 + V_m)/5)}, \\
\tau_{x_{r1}}(V_m) &= \frac{450}{1 + \exp((-45 - V_m)/10)} \frac{6}{1 + \exp((30 + V_m)/11.5)}, \\
x_{r1,\infty}(V_m) &= \frac{1}{1 + \exp((-26 - V_m)/7)}, \\
\tau_{x_{r2}}(V_m) &= \frac{3}{1 + \exp((-60 - V_m)/20)} \frac{1.12}{1 + \exp((-60 + V_m)/20)}, \\
x_{r2,\infty}(V_m) &= \frac{1}{1 + \exp((88 + V_m)/24)}.
\end{aligned}$$

The evolution of the gating variable f_{Ca} is also given by a Hodgkin-Huxley type equation, depending on Ca_{ss} . We have

$$\tau_{f_{Ca}}(Ca_{ss}) = \frac{80}{1 + \left(\frac{Ca_{ss}}{0.05}\right)^2} + 2, \quad f_{Ca,\infty}(Ca_{ss}) = \frac{0.6}{1 + \left(\frac{Ca_{ss}}{0.05}\right)^2} + 0.4.$$

Computing $\alpha(V_m)$ and $\beta(V_m)$. In the cell model of ten Tusscher we have 11 variables to describe the gating mechanism. For two of them we know $\alpha(V_m)$ and $\beta(V_m)$ from definition. For all others we have to compute the values if we want to know them. For the implemented numerical method the exact integrators it is sufficient to know τ_x and x_∞ . To use another numerical scheme we need the values of $\alpha(V_m)$ and $\beta(V_m)$. For a fixed potential V we have $\tau_x := \tau_x(V)$ and $x_\infty := x_\infty(V)$. With those we want to compute $\alpha := \alpha(V)$ and $\beta := \beta(V)$. To repeat shortly we know

$$\tau_x = \frac{1}{\alpha + \beta}$$

$$x_\infty = \frac{\alpha}{\alpha + \beta}.$$

Then

$$x_\infty = \alpha\tau_x \Leftrightarrow \alpha = \frac{x_\infty}{\tau_x}$$

and for β we have

$$\tau_x = \frac{1}{\alpha + \beta} \Leftrightarrow \tau_x(\alpha + \beta) = 1 \Leftrightarrow \beta = \frac{1}{\tau_x} - \alpha.$$

Inserting α gives

$$\beta = \frac{1}{\tau_x} - \frac{x_\infty}{\tau_x} = \frac{1 - x_\infty}{\tau_x}.$$

6. THE COURTEMANCHE CELL MODEL

In the atria, we use the Courtemanche cell model [Courtemanche et al., 1998]. Here, the model involves the ion concentration of calcium Ca , Ca_{up} , Ca_{rel} , sodium Na , and potassium K , and 15 gating variables

$$w = (Ca, Ca_{up}, Ca_{rel}, Na, K, m, h, j, o_a, o_i, u_a, u_i, x_r, x_s, d, f, f_{Ca}, u, v, w_{rel}),$$

and it depends on the constants g_{Na} , g_{CaL} , V_{CaL} , g_{Ks} , g_{to} , g_{Kr} , V_{Kr1} , V_{Kr2} , g_{K1} , V_{K1} , $I_{NaCa(max)}$, Ca_e , Na_e , $K_{m,Na(e)}$, $K_{m,Ca}$, k_{sat} , γ , F , R , T , $I_{NaK(max)}$, $K_{m,Na}$, K_e , K_{m,K_e} , $I_{p,Ca(max)}$, g_{bCa} , K_{Q10} and g_{bNa} for ionic currents and the constants V_i , $Ca_{up,max}$, k_{up} , k_{rel} , $I_{up(max)}$, $Trpn_{max}$, $Cmdn_{max}$, $Csqn_{max}$, $K_{m,Csqn}$, $K_{m,Cmdn}$, $K_{m,Trpn}$, cf. Tab. 3.

In the equation for the potential $C_m \partial_t V_m = I_{ion}(V_m, w) + I_{ext}$, the transmembrane current density I_{ion} given by

$$\begin{aligned} I_{ion}(V_m, w) = & I_{Na}(V_m, Na, m, h, j) + I_{CaL}(V_m, d, f, f_{Ca}) + I_{Ks}(V_m, K, x_s) + I_{to}(V_m, K, o_a, o_i) \\ & + I_{Kr}(V_m, K, x_r) + I_{Kur}(V_m, K, u_a, u_i) + I_{K1}(V_m, K) + I_{NaCa}(V_m, Na, Ca) \\ & + I_{NaK}(V_m, Na) + I_{pCa}(Ca) + I_{bCa}(V_m, Ca) + I_{bNa}(V_m, Na) \end{aligned}$$

combines the contribution of different ions, where

$$\begin{aligned}
I_{\text{Na}}(V_m, \text{Na}, m, h, j) &= g_{\text{Na}} m^3 h j (V_m - E_{\text{Na}}(\text{Na})) , \\
I_{\text{CaL}}(V_m, d, f, f_{\text{Ca}}) &= g_{\text{CaL}} d f f_{\text{Ca}} (V_m - V_{\text{CaL}}) , \\
I_{\text{Ks}}(V_m, \text{K}, x_s) &= g_{\text{Ks}} x_s^2 (V_m - E_{\text{K}}(\text{K})) , \\
I_{\text{to}}(V_m, \text{K}, o_a, o_i) &= g_{\text{to}} o_a^3 o_i (V_m - E_{\text{K}}(\text{K})) , \\
I_{\text{Kr}}(V_m, \text{K}, x_r) &= \frac{g_{\text{Kr}} x_r (V_m - E_{\text{K}}(\text{K}))}{1 + \exp((V_m + V_{\text{Kr1}})/V_{\text{Kr2}})} , \\
I_{\text{K1}}(V_m, \text{K}) &= \frac{g_{\text{K1}} (V_m - E_{\text{K}}(\text{K}))}{1 + \exp(0.07(V_m + V_{\text{K1}}))} , \\
I_{\text{Kur}}(V_m, \text{K}, u_a, u_i) &= g_{\text{Kur}} u_a^3 u_i (V_m - E_{\text{K}}(\text{K})) , \\
I_{\text{NaCa}}(V_m, \text{Na}, \text{Ca}) &= \frac{I_{\text{NaCa(max)}} (\exp(\gamma \frac{V_m F}{RT})) \text{Na}^3 \text{Ca}_e - \exp((\gamma - 1) \frac{V_m F}{RT}) \text{Na}_e^3 \text{Ca}}{(K_{\text{m,Na(e)}}^3 + \text{Na}_e^3)(K_{\text{m,Ca}} + \text{Ca}_e)(1 + k_{\text{sat}} \exp((\gamma - 1) V_m \frac{F}{RT}))} , \\
I_{\text{NaK}}(V_m, \text{Na}) &= I_{\text{NaK(max)}} f_{\text{NaK}} \frac{1}{1 + (K_{\text{m,Na}}/\text{Na})^{1.5}} \frac{K_e}{K_e + K_{\text{m,K}_e}} , \\
I_{\text{pCa}}(\text{Ca}) &= I_{\text{p,Ca(max)}} \frac{\text{Ca}}{0.0005 + \text{Ca}} , \\
I_{\text{bCa}}(V_m, \text{Ca}) &= g_{\text{bCa}} (V_m - E_{\text{Ca}}(\text{Ca})) , \\
I_{\text{bNa}}(V_m, \text{Na}) &= g_{\text{bNa}} (V_m - E_{\text{Na}}(\text{Na}))
\end{aligned}$$

with the reverse potentials

$$\begin{aligned}
E_{\text{Ca}}(\text{Ca}) &= \frac{RT}{zF} \log \frac{\text{Ca}_e}{\text{Ca}} , \\
E_{\text{Na}}(\text{Na}) &= \frac{RT}{zF} \log \frac{\text{Na}_e}{\text{Na}} , \\
E_{\text{K}}(\text{K}) &= \frac{RT}{zF} \log \frac{K_e}{K} .
\end{aligned}$$

The evolution of ion concentration. We have

$$\begin{aligned}
\partial_t \text{Na} &= -\frac{1}{V_i F} \left(I_{\text{Na}}(V_m, \text{Na}, m, h, j) + I_{\text{bNa}}(V_m, \text{Na}) + 3I_{\text{NaK}}(V_m, \text{Na}) + 3I_{\text{NaCa}}(V_m, \text{Na}, \text{Ca}) \right) , \\
\partial_t \text{K} &= -\frac{1}{V_i F} \left(I_{\text{K1}}(V_m, \text{K}) + I_{\text{to}}(V_m, \text{K}, o_a, o_i) + I_{\text{Kr}}(V_m, \text{K}, x_r) \right. \\
&\quad \left. + I_{\text{Ks}}(V_m, \text{K}, x_s) - 2I_{\text{NaK}}(V_m, \text{Na}) + I_{\text{Kur}}(V_m, \text{K}, u_a, u_i) \right) , \\
\partial_t \text{Ca} &= \left(-\frac{I_{\text{bCa}}(V_m, \text{Ca}) + I_{\text{pCa}}(\text{Ca}) + I_{\text{CaL}}(V_m, d, f, f_{\text{Ca}}) - 2I_{\text{NaCa}}(V_m, \text{Na}, \text{Ca})}{2V_i F} \right. \\
&\quad \left. + \frac{V_{\text{up}}(I_{\text{up,leak}} - I_{\text{up}}) + I_{\text{rel}} V_{\text{rel}}}{V_i} \right) \left(1 + \frac{\text{Trpn}_{\text{max}} K_{\text{m,Trpn}}}{(\text{Ca} + K_{\text{m,Trpn}})^2} + \frac{\text{Cmdn}_{\text{max}} K_{\text{m,Cmdn}}}{(\text{Ca} + K_{\text{m,Cmdn}})^2} \right)^{-1} , \\
\partial_t \text{Ca}_{\text{up}} &= I_{\text{up}}(\text{Ca}) - I_{\text{up,leak}}(\text{Ca}_{\text{up}}) - I_{\text{tr}}(\text{Ca}_{\text{up}}, \text{Ca}_{\text{rel}}) \frac{V_{\text{rel}}}{V_{\text{up}}} , \\
\partial_t \text{Ca}_{\text{rel}} &= \left(I_{\text{tr}}(\text{Ca}_{\text{up}}, \text{Ca}_{\text{rel}}) - I_{\text{rel}}(\text{Ca}, \text{Ca}_{\text{rel}}, u, v, w_{\text{rel}}) \right) \left(1 + \frac{\text{Csqn}_{\text{max}} K_{\text{m,Csqn}}}{(\text{Ca}_{\text{rel}} + K_{\text{m,Csqn}})^2} \right)^{-1}
\end{aligned}$$

with

$$\begin{aligned}
I_{\text{up}}(\text{Ca}) &= \frac{I_{\text{up}(\text{max})}}{1 + \frac{k_{\text{up}}}{\text{Ca}}} , \\
I_{\text{up,leak}}(\text{Ca}_{\text{up}}) &= \frac{\text{Ca}_{\text{up}}}{\text{Ca}_{\text{up,max}}} I_{\text{up}(\text{max})} , \\
I_{\text{tr}}(\text{Ca}_{\text{up}}, \text{Ca}_{\text{rel}}) &= \frac{\text{Ca}_{\text{up}} - \text{Ca}_{\text{rel}}}{180} , \\
I_{\text{rel}}(\text{Ca}, \text{Ca}_{\text{rel}}, u, v, w_{\text{rel}}) &= k_{\text{rel}} u^2 v w_{\text{rel}} (\text{Ca}_{\text{rel}} - \text{Ca}) .
\end{aligned}$$

The gating evolution in the Courtemanche model. For the evolution of the gating variables we specify every component of w independently. Every gating variable $y \in \{m, h, j, o_a, o_i, u_a, u_i, x_r, x_s, d, f, f_{\text{Ca}}, u, v, w_{\text{rel}}\}$ is described by a Hodgkin-Huxley type equation as given in (5), so that the evolution is determined by τ_y and y_∞ , cf. Sect. 5. As in the cell model of ten Tusscher all expressions depending on V_m are given in mV, i.e., in $\exp((V_m + 80)/6.8)$ the qualities 80 and 6.8 have the physical unit mV.

Here, we use for the gating variables $\{m, h, j\}$

$$\begin{aligned}
\tau_y(V_m) &= \frac{1}{a_y(V_m) + b_y(V_m)} , \\
y_\infty(V_m) &= a_y(V_m) b_y(V_m) ,
\end{aligned}$$

with

$$\begin{aligned}
a_m(V_m) &= \begin{cases} 3.2 & V_m = -47.13 , \\ 0.32 \frac{V_m + 47.13}{1 - \exp(-0.1(47.13 + V_m))} & \text{else} , \end{cases} \\
b_m(V_m) &= 0.08 \exp\left(-\frac{V_m}{11}\right) ,
\end{aligned}$$

$$\begin{aligned}
a_h(V_m) &= \begin{cases} 0 & V_m \geq -40 , \\ 0.135 \exp(-(V_m + 80)/6.8) & \text{else} , \end{cases} \\
b_h(V_m) &= \begin{cases} \left(0.13(1 + \exp(-(10.66 + V_m)/11.1))\right)^{-1} & V_m \geq -40 , \\ 3.56 \exp(0.079V_m) + 3.1 \cdot 10^5 \exp(0.35V_m) & \text{else} , \end{cases}
\end{aligned}$$

and

$$\begin{aligned}
a_j(V_m) &= \begin{cases} 0 & V_m \geq -40 , \\ \frac{(-127.14 \exp(0.2444V_m) - 3.474 \cdot 10^{-5} \exp(-0.04391V_m))(37.78 + V_m)}{1 + \exp(0.311(79.23 + V_m))} & \text{else} , \end{cases} \\
b_j(V_m) &= \begin{cases} 0.3 \frac{\exp(-2.535 \cdot 10^{-7}V_m)}{1 + \exp(-0.1(V_m + 32))} & V_m \geq -40 , \\ 0.1212 \frac{\exp(-0.01052V_m)}{1 + \exp(-0.1378(V_m + 40.14))} & \text{else} , \end{cases}
\end{aligned}$$

For the gating variables $\{o_a, o_i, u_a, u_i, x_r, x_s, d, f, w_{\text{rel}}\}$ we use

$$\tau_{o_a}(V_m) = \left(K_{Q10} \left(\frac{0.65}{\exp(-(10 + V_m)/8.5) + \exp(-(-30 + V_m)/59)} + \frac{0.65}{2.5 + \exp((82 + V_m)/17)} \right) \right)^{-1},$$

$$o_{a,\infty}(V_m) = \left(1 + \exp(-(20.47 + V_m)/17.54) \right)^{-1},$$

$$\tau_{o_i}(V_m) = \left(K_{Q10} \left(\frac{1}{18.53 + \exp((113.7 + V_m)/10.95)} + \frac{1}{35.56 + \exp(-(1.26 + V_m)/7.44)} \right) \right)^{-1},$$

$$o_{i,\infty}(V_m) = \left(1 + \exp((43.1 + V_m)/5.3) \right)^{-1},$$

$$\tau_{u_a}(V_m) = \tau_{o_a}(V_m),$$

$$u_{a,\infty}(V_m) = \left(1 + \exp(-(30.3 + V_m)/9.6) \right)^{-1},$$

$$\tau_{u_i}(V_m) = \left(K_{Q10} \left(\frac{1}{21 + \exp(-(-185 + V_m)/28)} + \exp((-158 + V_m)/16) \right) \right)^{-1},$$

$$u_{i,\infty}(V_m) = \left(1 + \exp((-99.45 + V_m)/27.48) \right)^{-1},$$

$$\tau_{x_r}(V_m) = \left(0.0003 \frac{14.1 + V_m}{1 - \exp(-(14.1 + V_m)/5)} + 7.3898 \cdot 10^{-5} \frac{-3.3328 + V_m}{\exp((-3.3328 + V_m)/5.1237) - 1} \right)^{-1},$$

$$x_{r,\infty}(V_m) = \left(1 + \exp(-(14.1 + V_m)/6.5) \right)^{-1},$$

$$\tau_{x_s}(V_m) = 0.5 \left(4 \cdot 10^{-5} \frac{-19.9 + V_m}{1 - \exp(-(-19.9 + V_m)/17)} + 3.5 \cdot 10^{-5} \frac{-19.9 + V_m}{\exp((-19.9 + V_m)/9) - 1} \right)^{-1},$$

$$x_{s,\infty}(V_m) = \left(1 + \exp(-(-19.9 + V_m)/12.7) \right)^{-\frac{1}{2}},$$

$$\tau_d(V_m) = \frac{1 - \exp(-(10 + V_m)/6.24)}{0.035(10 + V_m)(1 + \exp(-(10 + V_m)/6.24))},$$

$$d_{\infty}(V_m) = \left(1 + \exp(-(10 + V_m)/8) \right)^{-1},$$

$$\tau_f(V_m) = \frac{9}{0.0197 \exp(-0.0337^2(10 + V_m)^2) + 0.02},$$

$$f_{\infty}(V_m) = \left(1 + \exp((28 + V_m)/6.9) \right)^{-1},$$

$$\tau_{w_{\text{rel}}}(V_m) = 6 \frac{1 - \exp(-(-7.9 + V_m)/5)}{(-7.9 + V_m)(1 + 0.3 \exp(-(-7.9 + V_m)/5))},$$

$$w_{\text{rel},\infty}(V_m) = 1 - \left(1 + \exp(-(-40 + V_m)/17)\right)^{-1}.$$

For the gating variables $\{u, v\}$ we use

$$\tau_u = 8,$$

$$u_\infty(V_m, \text{Na}, d, f, f_{\text{Ca}}) = \left(1 + \exp\left(\frac{F_n(V_m, \text{Na}, d, f, f_{\text{Ca}}) - 3.4175 \cdot 10^{-13}}{13.67 \cdot 10^{-16}}\right)\right)^{-1},$$

$$\tau_v(V_m, \text{Na}, d, f, f_{\text{Ca}}) = 1.91 + 2.09 \left(1 + \exp\left(-\frac{F_n(V_m, \text{Na}, d, f, f_{\text{Ca}}) - 3.4175 \cdot 10^{-13}}{13.67 \cdot 10^{-16}}\right)\right)^{-1},$$

$$v_\infty(V_m, \text{Na}, d, f, f_{\text{Ca}}) = 1 - \left(1 + \exp\left(\frac{F_n(V_m, \text{Na}, d, f, f_{\text{Ca}}) - 6.835 \cdot 10^{-14}}{13.67 \cdot 10^{-16}}\right)\right)^{-1},$$

with

$$F_n(V_m, \text{Na}, d, f, f_{\text{Ca}}) = 10^{-12} V_{\text{rel}} I_{\text{rel}} - \frac{5 \cdot 10^{-13}}{F} \left(0.5 I_{\text{CaL}}(V_m, d, f, f_{\text{Ca}}) - 0.2 I_{\text{NaCa}}(V_m, \text{Na}, \text{Ca})\right)$$

and the function

$$g_{\text{Kur}}(V_m) = 0.005 + \frac{0.05}{1 + \exp(-(-15 + V_m)/13)}.$$

Finally, the evolution of the gating variable f_{Ca} is also given by a Hodgkin-Huxley type equation, depending on Ca. We have

$$\tau_{f_{\text{Ca}}} = 2,$$

$$f_{\text{Ca},\infty}(\text{Ca}) = \left(1 + \frac{\text{Ca}}{0.00035}\right)^{-1}.$$

7. A MODEL FOR CARDIAC ELECTROMECHANICS

We consider the human heart to be a bounded reference domain Ω , which is deformed into the current configuration by a *deformation* $\varphi: [0, T] \times \Omega \longrightarrow \mathbb{R}^3$ during one heartbeat ($T \approx 1s$). We set $\Omega_t = \varphi(t, \Omega)$.

The deformation φ is computed from the *displacement* $\mathbf{u}: [0, T] \times \Omega \longrightarrow \mathbb{R}^3$ by

$$\varphi(t, x) = \mathbf{x} + \mathbf{u}(t, x),$$

the elastic response depends on the *deformation gradient*

$$\mathbf{F}(t, x) := \mathbf{D}\varphi(t, x) = \left(\frac{\partial}{\partial x_i} \varphi_j(t, x)\right)_{i,j=1,\dots,3}.$$

From the separation of φ , we get $\mathbf{F} = \mathbf{I} + \mathbf{D}\mathbf{u}$, and we set $J = \det(\mathbf{F})$.

We use the balance equation in the *Lagrange configuration*

$$\varrho_0 \partial_t^2 \mathbf{u} = \text{div } \mathbf{P} \tag{7a}$$

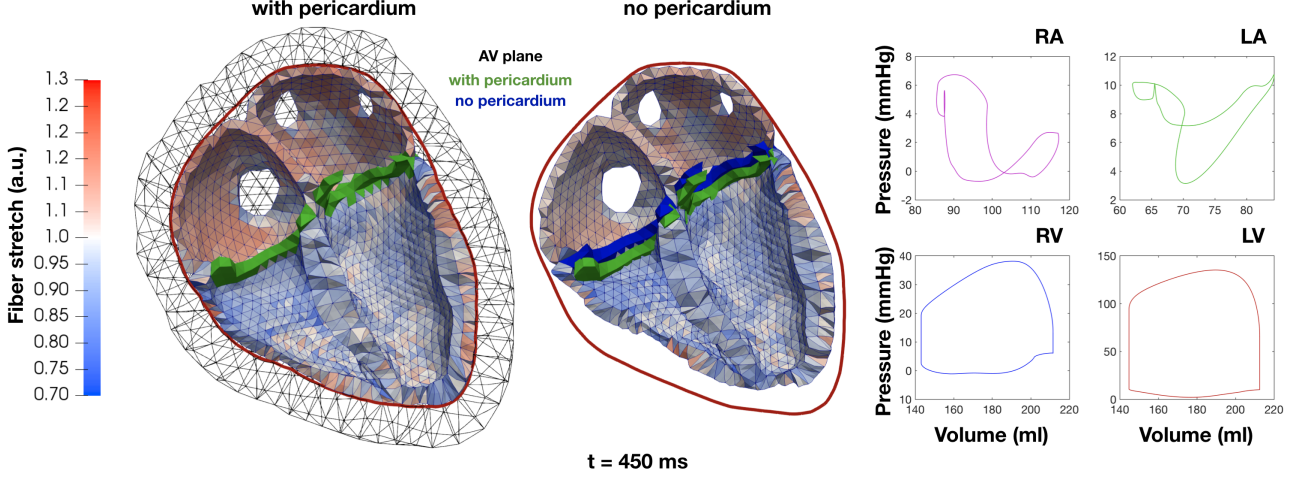


FIGURE 4. Reference geometry approximating ventricles and atria on level $\ell = 0$ and with three uniform refinement steps.

with reference density ϱ_0 and the stress \mathbf{P} depending on \mathbf{F} and an active strain or active stress model. This is complemented by boundary conditions on $\partial\Omega = \Gamma_D \cup \Gamma_P \cup \Gamma_{LV} \cup \Gamma_{RV} \cup \Gamma_{LA} \cup \Gamma_{RA}$ with Dirichlet boundary Γ_D , pericardium $\Gamma_P = \partial\Omega_T \cap \partial\Omega_V$, and boundaries $\Gamma_{LV} = \partial\Omega_V \cap \partial\Omega_{LV}$, $\Gamma_{RV} = \partial\Omega_V \cap \partial\Omega_{RV}$, $\Gamma_{LA} = \partial\Omega_A \cap \partial\Omega_{LA}$, $\Gamma_{RA} = \partial\Omega_A \cap \partial\Omega_{RA}$ of the left and right ventricular and atria chambers $\Omega_{LV}, \Omega_{RV}, \Omega_{LA}, \Omega_{RA}$, see Fig. 4.

We use the boundary conditions

$$\varphi = \mathbf{0}, \quad \text{on } \Gamma_D, \quad (7b)$$

$$[\varphi] = \mathbf{0}, \quad \text{on } \Gamma_P, \quad (7c)$$

$$\mathbf{P}\mathbf{n} = -p_{LV}\mathbf{n}, \quad \text{on } \Gamma_{LV}, \quad (7d)$$

$$\mathbf{P}\mathbf{n} = -p_{RV}\mathbf{n}, \quad \text{on } \Gamma_{RV}, \quad (7e)$$

$$\mathbf{P}\mathbf{n} = -p_{LA}\mathbf{n}, \quad \text{on } \Gamma_{LA}, \quad (7f)$$

$$\mathbf{P}\mathbf{n} = -p_{RA}\mathbf{n}, \quad \text{on } \Gamma_{RA}. \quad (7g)$$

Hyperelasticity. We assume cardiovascular tissue to be hyperelastic, i.e., there exists a stored energy function $W = W(\mathbf{F})$ which defines the stress response (in case of no active forces) by

$$\mathbf{P} = DW(\mathbf{F}).$$

Since the material is frame-indifferent, \tilde{W} exists such that $W(\mathbf{F}) = \tilde{W}(\mathbf{C})$, where $\mathbf{C} = \mathbf{F}^\top \mathbf{F}$ is left Cauchy Green strain tensor. Alternatively, the energy functional is given in the form $W(\mathbf{F}) = \tilde{W}(\mathbf{E})$ for $\mathbf{E} = \frac{1}{2}(\mathbf{C} - \mathbf{I})$, or $W(\mathbf{F}) = \tilde{W}(\boldsymbol{\iota}_\mathbf{C})$ depending on invariants $\boldsymbol{\iota}_\mathbf{C}$ of the strain tensor.

Anisotropy. In isotropic materials, the hyperelastic energy only depends on the *invariants* of \mathbf{C}

$$\iota_1(\mathbf{C}) = \text{trace}(\mathbf{C}), \quad \iota_2(\mathbf{C}) = \text{trace}(\text{Cof}(\mathbf{C})), \quad \iota_3(\mathbf{C}) = \det(\mathbf{C}) = J^2.$$

The cardiac tissue is strongly anisotropic. Depending on the fiber direction and the normal direction in the reference domain

$$\begin{aligned}\mathbf{f}: \Omega &\longrightarrow S^2, \\ \mathbf{n}: \Omega &\longrightarrow S^2\end{aligned}$$

with $\mathbf{n} \cdot \mathbf{f} = 0$ we define $\mathbf{s} = \mathbf{f} \times \mathbf{n}$. This defines the *anisotropic invariants*

$$\begin{aligned}\iota_{4,\mathbf{f}}(\mathbf{C}) &= \mathbf{f} \cdot \mathbf{C}\mathbf{f}, \\ \iota_{4,\mathbf{n}}(\mathbf{C}) &= \mathbf{n} \cdot \mathbf{C}\mathbf{n}, \\ \iota_{4,\mathbf{s}}(\mathbf{C}) &= \mathbf{s} \cdot \mathbf{C}\mathbf{s}, \\ \iota_{8,\mathbf{fs}}(\mathbf{C}) &= |\mathbf{f} \cdot \mathbf{C}\mathbf{s}|.\end{aligned}$$

Constitutive models. With the representation above, we now specify the hyperelastic energy. For cardiac tissue, several models are proposed to imitate its viscoelastic behaviour. Commonly used models are:

- (1) **Neo-Hooke model.** One of the simplest non-linear material models is given by

$$\tilde{W}(\mathbf{C}) = \frac{\mu}{2}(\text{trace}(\mathbf{C}) - 3) + \Gamma_\lambda(J), \quad \Gamma_\lambda(J) = \frac{\lambda}{2}(J - 1)^2$$

with parameters μ and λ . Though it is easy to implement, it does not capture the anisotropy of cardiac tissue.

- (2) **Guccione model.** An early contribution to anisotropic material models was given in [Guccione et al., 1991], defining the *Guccione material*

$$\check{W}(\mathbf{E}) = \frac{C_0}{2} \exp[Q_{\mathbf{f},\mathbf{s}}(\mathbf{E}) - 1] + \Gamma_\lambda(J)$$

with parameters C_0 , μ and λ and $Q_{\mathbf{f},\mathbf{s}}(\mathbf{E})$ defining the functional

$$Q_{\mathbf{f},\mathbf{s}}(\mathbf{E}) := b_1 \bar{E}_{11}^2 + b_2(\bar{E}_{22}^2 + \bar{E}_{33}^2 + \bar{E}_{23}^2 + \bar{E}_{32}^2) + b_3(\bar{E}_{12}^2 + \bar{E}_{21}^2 + \bar{E}_{13}^2 + \bar{E}_{31}^2),$$

where

$$\bar{E} = \mathbf{f} \cdot \mathbf{E}\mathbf{f} + \mathbf{s} \cdot \mathbf{E}\mathbf{s} + \mathbf{n} \cdot \mathbf{E}\mathbf{n}$$

is the Green strain tensor oriented along the fibre direction. The parameters b_1, b_2, b_3 are determined by experiments.

- (3) **Holzappel-Ogden model.** We use the general energy proposed by [Holzapfel and Ogden, 2009] defining a *Holzappel-Ogden material*:

$$\begin{aligned}\mathring{W}(\mathbf{C}) &= \frac{a}{2b} [\exp(b(\iota_1(\mathbf{C}) - 3)) - 1] + \frac{a_{\mathbf{f}}}{2b_{\mathbf{f}}} [\exp(b_{\mathbf{f}}(\iota_{4,\mathbf{f}}(\mathbf{C}) - 1)^2) - 1] \\ &\quad + \frac{a_{\mathbf{s}}}{2b_{\mathbf{s}}} [\exp(b_{\mathbf{s}}(\iota_{4,\mathbf{s}}(\mathbf{C}) - 1)^2) - 1] + \frac{a_{\mathbf{fs}}}{2b_{\mathbf{fs}}} [\exp(b_{\mathbf{fs}}\iota_{8,\mathbf{fs}}(\mathbf{C})^2) - 1] + \Gamma_\lambda(J)\end{aligned}$$

with parameters $a, b, a_{\mathbf{f}}, b_{\mathbf{f}}, a_{\mathbf{s}}, b_{\mathbf{s}}, a_{\mathbf{fs}}, b_{\mathbf{fs}}$ determined by physical experiments.

The active strain decomposition. The conclusions above all rely on the assumption that soft tissue can be modeled as elastic. In reality, cardiac cells have viscoelastic behaviour. While rapid and repeated stretching causes a stiffening effect, the tissue loosens when exposed to prolonged elongation. Some of these effects are permanent, meaning that the pullback into Lagrange configuration would actually lead to a different, intermediate configuration. To account for this plasticity, we use the *active strain* model described in [Ambrosi et al., 2011, Rossi et al., 2012]. Separating the deformation gradient \mathbf{F} into an elastic, passive part \mathbf{F}_e and an active part \mathbf{F}_a , we write

$$\mathbf{F} = \mathbf{F}_e \mathbf{F}_a \quad (8)$$

The tensor \mathbf{F}_a accounts for the active deformation induced by the cells.

For each cell, we denote by $\gamma_{\mathbf{f}}, \gamma_{\mathbf{s}}, \gamma_{\mathbf{n}}: [0, T] \times \Omega \rightarrow \mathbb{R}$ their deformation into the respective direction $\mathbf{f}, \mathbf{s}, \mathbf{n}$. Setting

$$\mathbf{F}_a = \mathbf{I} + \gamma_{\mathbf{f}} \mathbf{f} \otimes \mathbf{f} + \gamma_{\mathbf{s}} \mathbf{s} \otimes \mathbf{s} + \gamma_{\mathbf{n}} \mathbf{n} \otimes \mathbf{n}, \quad (9)$$

we can make the following assumptions:

- Cardiac cells are transverse isotropic along \mathbf{f} , i.e. $\gamma_{\mathbf{s}} = \gamma_{\mathbf{n}}$.
- The cells consist mostly of water and are therefore isochoric, i.e., their volume is constant, so that $J_a := \det(\mathbf{F}_a) = 1$.

From these two conditions follows directly that

$$\det(\mathbf{F}_a) = (\gamma_{\mathbf{f}} + 1)(\gamma_{\mathbf{s}} + 1)^2 = 1$$

and therefore $\gamma_{\mathbf{s}} = \frac{1}{\sqrt{\gamma_{\mathbf{f}} + 1}} - 1$. Hence we only need to compute $\gamma_{\mathbf{f}}$. We then set a new stress response

$$\mathbf{P} = \mathbf{D}_{\mathbf{F}} W(\mathbf{F} \mathbf{F}_a^{-1}),$$

which allows a pullback into the actual Lagrange configuration. An in-depth explanation of the evolution of $\gamma_{\mathbf{f}}$ is given in Sect. 8.

Within this active strain model, we need to recompute the invariants as they now depend on $\gamma_{\mathbf{f}}$, i.e.

$$\iota_1^e = (1 + \gamma_{\mathbf{f}}) \iota_1 - \left((\gamma_{\mathbf{f}} + \gamma_{\mathbf{f}} \frac{\gamma_{\mathbf{f}} + 2}{(1 + \gamma_{\mathbf{f}})^2}) \right) \iota_{4,\mathbf{f}}$$

and

$$\iota_{4,\mathbf{f}}^e = (1 + \gamma_{\mathbf{f}})^{-2} \iota_{4,\mathbf{f}}, \quad \iota_{4,\mathbf{s}}^e = (1 + \gamma_{\mathbf{f}}) \iota_{4,\mathbf{s}}, \quad \iota_{8,\mathbf{fs}}^e = (1 + \gamma_{\mathbf{f}})^{-\frac{1}{2}} \iota_{8,\mathbf{fs}}.$$

The active stress decomposition. An alternative approach to the multiplicative split of the deformation, as described above, is to additively split the stress tensor

$$\mathbf{P} = \mathbf{D}_{\mathbf{F}} W(\mathbf{F}) + T_{\max} T_{\text{tot}}(w, g) \mathbf{f}^{\varphi} \otimes \mathbf{f}^{\varphi}, \quad (10)$$

where T_{\max} is a constant adjusting for the maximal active tension and T_{tot} the current tension generated by cellular evolution model, cf. Sect. 8.

The Newmark method. Now that we know how to properly calculate $\mathbf{P}(\mathbf{D}\varphi, w)$, a proper time-integration strategy is needed to solve the dynamic system (7). We implement a *Newmark β -scheme* [Crisfield, 1997], where at each time step n we solve for $\mathbf{u}(t_n, \mathbf{x}) = \mathbf{u}^n$, approximating $\partial_t^2 \mathbf{u} \approx \mathbf{a}^n$ with

$$\mathbf{u}^n = \mathbf{u}^{n-1} + \Delta t \mathbf{v}^{n-1} + (\Delta t)^2 \left(\frac{1 - 2\beta_N}{2} \mathbf{a}^{n-1} + \beta_N \mathbf{a}^n \right), \quad (11a)$$

$$\mathbf{v}^n = \mathbf{v}^{n-1} + \Delta t ((1 - \gamma_N) \mathbf{a}^{n-1} + \gamma_N \mathbf{a}^n) \quad (11b)$$

and $\mathbf{a}^0 = \mathbf{0}$. The approximated dynamic system is the given by

$$\varrho_0 \mathbf{a}^n - \operatorname{div} \mathbf{P}(\mathbf{I} + \mathbf{D}\mathbf{u}^n) = 0. \quad (12)$$

Solving for \mathbf{a}^n in (11a) and replacing \mathbf{a}^n and \mathbf{v}^n in (12) gives us

$$\varrho_0 \left[\frac{1}{\beta_N \Delta t} \left(\frac{1}{\Delta t} (\mathbf{u}^n - \mathbf{u}^{n-1}) - \mathbf{v}^{n-1} \right) - \frac{1 - 2\beta_N}{2\beta_N} \mathbf{a}^{n-1} \right] - \operatorname{div} \mathbf{P}(\mathbf{I} + \mathbf{D}\mathbf{u}^n) = \mathbf{0}. \quad (13)$$

The standard Newmark parameters are $\beta_N = 0.25$ and $\gamma_N = 0.5$. As these values dictate the damping of the system, further combinations are being tested in our experiments.

The ventricle volume. The reference domains for each chamber C are given by Ω_{LV} , Ω_{RV} , Ω_{LA} , Ω_{RA} . The volume of the deformed chambers are then denoted by $|\Omega_{LV}^\varphi|$, $|\Omega_{RV}^\varphi|$, $|\Omega_{LA}^\varphi|$, $|\Omega_{RA}^\varphi|$, and would be computed by

$$|\Omega_C^\varphi| = \int_{\Omega_C^\varphi} 1 d\mathbf{x}, \quad C \in \{LV, RV, LA, RA\}.$$

On the discrete geometry however, the chamber volumes are evaluated by the sum of volumes of all tetrahedrons constructed by a surface triangle $K \subset \partial\Omega_C$ and the center point \mathbf{x}_C . By denoting the vectors of the vertices of K by \mathbf{a}_K , \mathbf{b}_K , \mathbf{c}_K , we obtain

$$|\Omega_C^\varphi| \approx \sum_{K \subset \partial\Omega_C} \frac{1}{6} (\mathbf{a}_K - \mathbf{x}_C) \cdot ((\mathbf{b}_K - \mathbf{a}_K) \times (\mathbf{c}_K - \mathbf{a}_K)).$$

8. THE CELL-CONTRACTION MODEL

The cell-contraction model for the active strain approach used in Sect. 7 involves two parts: The stretch model itself and a second model simulating an active tension depending on the current concentration of Calcium. Together, it determines the stretch $\gamma_{\mathbf{f}}$ depending on the deformation, on the calcium concentration in the set of variables w for the cell model, and on an additional set of gating variables g for the tension model.

The contraction model determines the stretch $\gamma_{\mathbf{f}}$ and involves a set of 9 gating variables

$$g = (\operatorname{Tr}, B, U, W, S, \zeta_W, \zeta_S, C_s, C_d).$$

The evolution of the stretch depends on the deformation gradient $\mathbf{D}\boldsymbol{\varphi}$, the fiber direction \mathbf{f} , and the parameters l_0 , l_{\min} , l_{\max} , c_0 , c_k , d_k ($k = 1, 2, 3$) [Ruiz-Baier et al., 2014], cf. Tab. 5. The gating mechanism determines the total force $T_{\text{tot}}(w, g)$ and depends on the constants k_{Tr} , n_{Tr} , $\text{Ca}_{\text{T50}}^{\text{ref}}$, k_B , $n_{\text{Tr}B}$, k_{UW} , k_{WS} , r_W , r_S , γ_W , γ_S , ϕ , A_{eff} , β_0 , β_1 , T_{ref} , cf. Tab. 4.

The Stretch Model. The stretch value $\gamma_{\mathbf{f}}$ is determined a nonlinear ODE

$$\partial_t \gamma_{\mathbf{f}} = G_{\gamma_{\mathbf{f}}}(\gamma_{\mathbf{f}}, \mathbf{D}\boldsymbol{\varphi}, \mathbf{f}, g, w) \quad (14a)$$

We use the model [Quarteroni et al., 2017] given by

$$G_{\gamma_{\mathbf{f}}}(\gamma_{\mathbf{f}}, \mathbf{D}\boldsymbol{\varphi}, \mathbf{f}, g, w) = \frac{1}{\eta_a} \left[\left(\mathbf{D}_{\iota_1^e} W(\mathbf{F}_e) + \mathbf{D}_{\iota_{4,\mathbf{f}}^e} W(\mathbf{F}_e) \right) \left(\hat{F}_a(w, g, \iota_{4,\mathbf{f}}, \gamma_{\mathbf{f}}) - \frac{2\iota_{4,\mathbf{f}}}{(1 + \gamma_{\mathbf{f}})^3} \right) - \mathbf{f} \cdot \mathbf{D}_{\mathbf{F}_a} W(\mathbf{F}_e) \mathbf{f} \right]$$

depending on geometrical quantities and the calcium concentration Ca

$$\hat{F}_a(w, g, \iota_{4,\mathbf{f}}, \gamma_{\mathbf{f}}) = \alpha T_{\text{tot}}(w, g) R_{\text{F-L}}(\iota_{4,\mathbf{f}}, \gamma_{\mathbf{f}}), \quad (14b)$$

where \hat{F}_a is the active tension created in the cardiac cells depending on the concentration of Ca^{2+} -Ions and the invariant of the their current deformation $\iota_{4,\mathbf{f}}$. Note that only the invariant along \mathbf{f} is needed, as the cardiac force mechanism is modeled in 1D. The evaluation of the resulting force T_{tot} and the force-length relationship $R_{\text{F-L}}$ depends on the used force model of the cells. The model for T_{tot} is described in the next section, and $R_{\text{F-L}}$ is approximated by fitted Taylor Series

$$R_{\text{F-L}}(\iota_{4,\mathbf{f}}) = \chi_{[l_{\min}, l_{\max}]}(l_0 + \gamma_{\mathbf{f}}) \left[\frac{c_0}{2} + \sum_{k=1}^3 \left(c_k \sin(kl_0 \iota_{4,\mathbf{f}}) + d_k \cos(kl_0 \iota_{4,\mathbf{f}}) \right) \right], \quad \chi_{[a,b]}(x) = \begin{cases} 1 & x \in [a, b], \\ 0 & x \notin [a, b]. \end{cases}$$

The Land Tension Cell Model. To model the tension generated by activated cardiac muscle cells, we use the model described by Land et al. [Land et al., 2017]. It simulates cardiac myocytes using ion concentrations of calcium (Ca) and troponin (Tr) as well as crossbridge binding of sarcomeres using a three-state crossbridge cycle

$$\partial_t \text{Tr} = k_{\text{Tr}} \left[\left(\frac{\text{Ca}}{\text{Ca}_{\text{T50}}} \right)^{n_{\text{Tr}}} (1 - \text{Tr}) - \text{Tr} \right] \quad (15)$$

Here, Tr represents the fraction of troponin units with calcium bond. This concentration drives the unblocking of tropomyosin. The fraction of blocked binding sites (B) is given by

$$\partial_t B = k_B \cdot \text{Tr}^{\frac{-n_{\text{Tr}B}}{2}} U - k_U \cdot \text{Tr}^{\frac{n_{\text{Tr}B}}{2}} B \quad (16)$$

The following crossbridge cycle contains an unbound (U), a pre-powerstroke (W) and a post-powerstroke (S) state. They are given by the relation

$$U = (1 - B) - S - W, \quad (17a)$$

$$\partial_t W = k_{UW}U - k_{WU}W - k_{WS}W - \gamma_{WU}W, \quad (17b)$$

$$\partial_t S = k_{WS}W - k_{SU}S - \gamma_{SU}S, \quad (17c)$$

with parameters k_{UW} , k_{WU} , k_{WS} , k_{SU} . The values of γ_{WU} and γ_{SU} are derived from the distortion-decay model

$$\partial_t \zeta_W = A_W \partial_t \lambda_{\mathbf{f}} - c_W \zeta_W \quad \partial_t \zeta_S = A_S \partial_t \lambda_{\mathbf{f}} - c_S \zeta_S \quad (18a)$$

$$\gamma_{WU} = \gamma_W |\zeta_W| \quad \gamma_{SU} = \begin{cases} -\gamma_S(\zeta_S + 1) & \text{if } \zeta_S < 1, \\ \gamma_S \zeta_S & \text{if } \zeta_S > 2, \\ 0 & \text{otherwise.} \end{cases} \quad (18b)$$

A_W and A_S relate to the magnitude of the instantaneous distortion response while c_W and c_S represent decay rates. The variable $\lambda_{\mathbf{f}}$ corresponds to the relative cell length, i.e. $\lambda_{\mathbf{f}} = \frac{l_0 + \gamma_{\mathbf{f}}}{l_0}$. As it is difficult to provide the values for k , A and c directly, we define the *steady-state ratios*

$$r_S = \text{steady-state} \frac{S}{U + W + S}, \quad (19a)$$

$$r_W = \text{steady-state} \frac{W}{U + W}. \quad (19b)$$

This allows for an easier parameter estimation and gives the following relations:

$$k_{WU} = k_{UW} \left(\frac{1}{r_W} - 1 \right) - k_{WS}, \quad (20a)$$

$$k_{SU} = k_{WS} r_W \left(\frac{1}{r_S} - 1 \right), \quad (20b)$$

$$k_B = k_U \frac{\text{Tr}^{n_{\text{TrB}}}}{1 - r_S - (1 - r_S)r_W}. \quad (20c)$$

We further assume the magnitude of instantaneous distortion in W and S are equal, i.e.

$$A_S = A_W = A_{\text{eff}} \frac{r_S}{(1 - r_S)r_W + r_S}. \quad (21)$$

Additionally, we view the distortion decay rates to be proportional to the steady-state crossbridge cycling rates:

$$c_W = \phi k_{UW} \frac{U}{W} = \phi k_{UW} \frac{(1 - r_S)(1 - r_W)}{(1 - r_S)r_W}, \quad (22a)$$

$$c_S = \phi k_{WS} \frac{W}{S} = \phi k_{WS} \frac{(1 - r_S)r_W}{r_S}. \quad (22b)$$

$$T_a = h(\lambda_f) \frac{T_{\text{ref}}}{r_S} ((\zeta_S + 1)S + \zeta_W W) \quad (23)$$

where T_{ref} is the maximal active tension at resting length and

$$h(\lambda_f) = \max \left\{ 0, \tilde{h}(\min\{\lambda_f, 1.2\}) - 1 \right\}, \quad (24a)$$

$$\tilde{h}(\lambda_f) = 1 + \beta_0 (\lambda_f + \min\{\lambda_f, 0.87\} - 1.87) \quad (24b)$$

enforces a length-dependency on the tension. Such a dependency is also introduced for the half-activation point Ca_{T50} used in equ. (15)

$$\text{Ca}_{T50} = \text{Ca}_{T50}^{\text{ref}} + \beta_1 (\min\{\lambda_f, 1.2\} - 1). \quad (25)$$

In the coupled model, we also need to account for a passive tension withing sarcomeres. A sufficient implementation of such a passive cell model is given by

$$C_s = (\lambda_f - 1) - C_d, \quad \partial_t C_d = k \frac{C_s}{\eta}, \quad \eta = \begin{cases} \eta_l & \text{if } C_s > 0, \\ \eta_s & \text{if } C_s \leq 0. \end{cases} \quad (26)$$

The passive tension is then calculated by

$$T_p = akC_s \quad (27)$$

and the resulting tension of the force model is given by

$$T_{\text{tot}} = T_a + T_p. \quad (28)$$

9. THE CIRCULATORY SYSTEM

The heart interacts with the human vascular system, see [Quarteroni et al., 2019] for the mathematical modelling of the human cardiovascular system, [Barbarotta et al., 2018] for a specific activation model for ventricular contraction, [Fedele et al., 2017] for an aortic valve model, and [Tagliabue et al., 2017] for an idealized blood flow model in the ventricle.

Here we use a lumped parameter model of the closed-loop human vascular system to include more realistic hemodynamic boundary conditions in our model of cardiac mechanics. This model is driven by the volume changes of the four chambers $|\Omega_{VL}^\varphi|, |\Omega_{VR}^\varphi|, |\Omega_{AL}^\varphi|, |\Omega_{AR}^\varphi|$, where the deformation φ depends on the pressure values of the right/left ventricular and right/left atrial chambers

$$p = (p_{VR}, p_{VL}, p_{VR}, p_{VL}).$$

The circulatory system is determines

$$z = (v_{SysVen}, v_{SysArt}, v_{PulVen}, v_{PulArt}, v_{VR}, v_{VL}, v_{VR}, v_{VL})$$

describing the systemic venous, systemic arterial, pulmonary venous, pulmonary arterial, right/left ventricular, and right/left atrial volumes, and depending on the parameters $R_{SysArtValve}$, R_{SysArt} , C_{SysArt} , $v_{SysArtUnstr}$, R_{SysPer} , R_{SysVen} , C_{SysVen} , $v_{SysVenUnstr}$, $R_{RavValve}$, $R_{PulArtValve}$, R_{PulArt} , C_{PulArt} , $v_{PulArtUnstr}$, R_{PulPer} , R_{PulVen} , C_{PulVen} , $v_{PulVenUnstr}$, and $R_{LavValve}$.

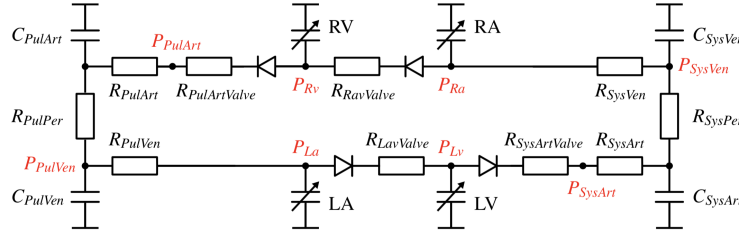


FIGURE 5. Schematic of the circulatory system model with the pressure values p , resistances R , and compliances C .

In this closed loop system, the evolution of z is determined by

$$\begin{aligned} \partial_t v_{VL} &= \max \left\{ \frac{p_{AL} - p_{VL}}{R_{LavValve}}, 0 \right\} - \max \left\{ \frac{p_{VL} - p_{CSysArt}}{R_{SysArtValve} + R_{SysArt}}, 0 \right\}, \\ \partial_t v_{SysVen} &= \frac{p_{CSysArt} - p_{SysVen}}{R_{SysPer}} - \frac{p_{SysVen} - p_{VR}}{R_{SysVen}}, \\ \partial_t v_{VR} &= \max \left\{ \frac{p_{VR} - p_{VR}}{R_{RavValve}}, 0 \right\} - \max \left\{ \frac{p_{VR} - p_{CPulArt}}{R_{PulArtValve} + R_{PulArt}}, 0 \right\}, \\ \partial_t v_{PulVen} &= \frac{p_{CPulArt} - p_{PulVen}}{R_{PulPer}} - \frac{p_{PulVen} - p_{VL}}{R_{PulVen}}, \\ \partial_t v_{SysArt} &= \max \left\{ \frac{p_{VL} - p_{CSysArt}}{R_{SysArtValve} + R_{SysArt}}, 0 \right\} - \frac{p_{CSysArt} - p_{SysVen}}{R_{SysPer}}, \\ \partial_t v_{VR} &= \frac{p_{SysVen} - p_{VR}}{R_{SysVen}} - \max \left\{ \frac{p_{VR} - p_{VR}}{R_{RavValve}}, 0 \right\}, \\ \partial_t v_{PulArt} &= \max \left\{ \frac{p_{VR} - p_{CPulArt}}{R_{PulArtValve} + R_{PulArt}}, 0 \right\} - \frac{p_{CPulArt} - p_{PulVen}}{R_{PulPer}}, \\ \partial_t v_{AL} &= \frac{p_{PulVen} - p_{VL}}{R_{PulVen}} - \max \left\{ \frac{p_{AL} - p_{VL}}{R_{LavValve}}, 0 \right\} \end{aligned}$$

subject to the relations for the pressure values

$$(p_{\text{SysVen}}, p_{\text{SysArt}}, p_{\text{PulVen}}, p_{\text{PulArt}})$$

for the systemic venous, systemic arterial, pulmonary venous, and pulmonary arterial pressures given by

$$\begin{aligned} p_{\text{CSysArt}} &= \frac{v_{\text{SysArt}}}{C_{\text{SysArt}}}, & p_{\text{SysVen}} &= \frac{v_{\text{SysVen}}}{C_{\text{SysVen}}}, \\ p_{\text{SysArt}} &= p_{\text{VL}} - R_{\text{SysArtValve}} \cdot \max \left\{ \frac{p_{\text{VL}} - p_{\text{CSysArt}}}{R_{\text{SysArtValve}} + R_{\text{SysArt}}}, 0 \right\}, \\ p_{\text{CPulArt}} &= \frac{v_{\text{PulArt}}}{C_{\text{PulArt}}}, & p_{\text{PulVen}} &= \frac{v_{\text{PulVen}}}{C_{\text{PulVen}}}, \\ p_{\text{PulArt}} &= p_{\text{VR}} - R_{\text{PulArtValve}} \cdot \max \left\{ \frac{p_{\text{VR}} - p_{\text{CPulArt}}}{R_{\text{PulArtValve}} + R_{\text{PulArt}}}, 0 \right\} \end{aligned}$$

and subject to the constraints

$$v_{\text{VL}} = |\Omega_{\text{VL}}^{\varphi}|, \quad v_{\text{VR}} = |\Omega_{\text{VR}}^{\varphi}|, \quad v_{\text{AL}} = |\Omega_{\text{AL}}^{\varphi}|, \quad v_{\text{AR}} = |\Omega_{\text{AR}}^{\varphi}|, \quad (29)$$

where the deformation φ depends on $p = (p_{\text{VR}}, p_{\text{VL}}, p_{\text{VR}}, p_{\text{VL}})$.

The incremental realization. Withing one time step of the mechanical problem, we first find an approximated pressure p through the closed-loop model. We either use a multistep method using previous pressure values, or simply add a fixed amount in each chamber during the first initialization steps.

Next, we update the mechanical and circulatory models and compare the resulting chamber volumes if the residuals $r_i = |\Omega_i^{\varphi}| - v_i$ for $i \in \{\text{VL}, \text{VR}, \text{AL}, \text{AR}\}$ are below a threshold ε_p . If they are, the pressure p is accepted and one moves to the next time step. Otherwise, we update p by a quasi Newton method:

$$p^n = p^{n-1} - \mathbf{C}_n^{-1} r^n, \quad (30)$$

where \mathbf{C}_n is the *compliance matrix* determined by

$$\mathbf{C}_n^{-1} = \mathbf{C}_{n-1}^{-1} + (\Delta p_n - \mathbf{C}_{n-1}^{-1} \Delta r_n) \frac{\Delta p_n^{\top} \mathbf{C}_{n-1}^{-1}}{\Delta p_n^{\top} \mathbf{C}_{n-1}^{-1} \Delta r_n} \quad (31)$$

with $\Delta p_n = p_n - p_{n-1}$, $\Delta r_n = r_n - r_{n-1}$.

APPENDIX A. MONODOMAIN PARAMETERS

The parameters and initial valuse for the monodomain model are given in Tab. 1.

TABLE 1. Parameters for the evolution of the electric potential in the monodomain equations.

surface-to-volume ratio	$\beta = 140 \text{ mm}^{-1}$
membrane capaticity	$C_m = 0.01 \text{ }\mu\text{Fmm}^{-1}$
longitudinal conductivity	$\sigma_{\text{A,l}} = 556.9188 \text{ Smm}^{-1}, \sigma_{\text{V,l}} = 133.4177215 \text{ Smm}^{-1} = \text{AV}^{-1}\text{mm}^{-1}$
transversal conductivity	$\sigma_{\text{A,t}} = 251.0 \text{ Smm}^{-1}, \sigma_{\text{V,t}} = 17.60617761 \text{ Smm}^{-1}$
initial potential ventricles	$V_m^0 = -80.8887 \text{ mV}$
initial potential atrim	$V_m^0 = -85.298 \text{ mV}$
external current ventricle	$V_e = 0.582155 \text{ nA}$
external current atrium	$V_e = 20 \text{ pApF}^{-1}$

For the ten Tuschler cell model, the parameters are given in Tab. 2, and initial values for the ion concentrations and gating variables

$$w^0 = (\text{Ca}^0, \text{Ca}_{\text{SS}}^0, \text{Ca}_{\text{SR}}^0, \text{Na}^0, \text{K}^0, \overline{R}^0, m^0, h^0, j^0, x_{\text{r1}}^0, x_{\text{r2}}^0, x_{\text{s}}^0, s^0, r^0, d^0, f^0, f_2^0, f_{\text{Ca}}^0, \overline{O}^0)$$

at $t = 0$ and for all $x \in \Omega_V$ are set to

$$\begin{aligned} \text{Ca}^0 &= 0.00011576, & \text{Ca}_{\text{SS}}^0 &= 0.000233, & \text{Ca}_{\text{SR}}^0 &= 4.1371, & \text{Na}^0 &= 9.4148, & \text{K}^0 &= 136.0009, & \overline{R}^0 &= 0.98738, \\ m^0 &= 0.0016901, & h^0 &= 0.74684, & j^0 &= 0.74622, & x_{\text{r1}}^0 &= 0.00021327, & x_{\text{r2}}^0 &= 0.4719, & x_{\text{s}}^0 &= 0.0033368, \\ s^0 &= 1, & r^0 &= 2.3886 \cdot 10^{-8}, & d^0 &= 3.3409 \cdot 10^{-5}, & f^0 &= 0.95972, & f_2^0 &= 0.99949, & f_{\text{Ca}}^0 &= 0.99996, \\ \overline{O}^0 &= 0. \end{aligned}$$

For the Courtemanche cell model, the parameters are given in Tab. 3, and initial values for the ion concentrations and gating variables

$$w^0 = (\text{Ca}^0, \text{Ca}_{\text{up}}^0, \text{Ca}_{\text{rel}}^0, \text{Na}^0, \text{K}^0, m^0, h^0, j^0, o_{\text{a}}^0, o_{\text{i}}^0, u_{\text{a}}^0, u_{\text{i}}^0, x_{\text{r}}^0, x_{\text{s}}^0, d^0, f^0, f_{\text{Ca}}^0, u^0, v^0, w_{\text{rel}}^0)$$

at $t = 0$ and for all $x \in \Omega_A$ are set to

$$\begin{aligned} \text{Ca}^0 &= 0.000112836, & \text{Ca}_{\text{up}}^0 &= 1.52919, & \text{Ca}_{\text{rel}}^0 &= 1.10817, & \text{Na}^0 &= 11.83, & \text{K}^0 &= 138.994, \\ m^0 &= 0.00304588, & h^0 &= 0.962696, & j^0 &= 0.975742, & o_{\text{a}}^0 &= 0.0309106, & o_{\text{i}}^0 &= 0.999163, \\ u_{\text{a}}^0 &= 0.00511314, & u_{\text{i}}^0 &= 0.986906, & x_{\text{r}}^0 &= 0.00229885, & x_{\text{s}}^0 &= 0.0196603, & d^0 &= 0.000141583, \\ f^0 &= 0.916064, & f_{\text{Ca}}^0 &= 0.75607, & u^0 &= 5.60519 \cdot 10^{-43}, & v^0 &= 0.999994, & w_{\text{rel}}^0 &= 0.999185. \end{aligned}$$

TABLE 2. Parameters in the ten Tuschler cell model.

gas constant	$R = 8314.472 \text{ mJK}^{-1}\text{mol}^{-1}$
temperature	$T = 310 \text{ K}$
Faraday constant	$F = 96485.3415 \text{ C/mol}$
valence of the ionic species	$z = 1 \text{ for Na and K, } z = 2 \text{ for Ca}$
$V_{m, \text{CaL}}$	15 mV
$V_{m, \text{pK}, 1}$	25 mV
$V_{m, \text{pK}, 2}$	5.98 mV
Extracellular K^+ concentration	$\text{K}_e = 5.4 \text{ mM}$
Extracellular Na^+ concentration	$\text{Na}_e = 140 \text{ mM}$
Extracellular Ca^{2+} concentration	$\text{Ca}_e = 2 \text{ mM}$
cytoplasmic volume	$V_c = 0.016404 \text{ mm}^3$
maximal I_{Na} conductance	$G_{\text{Na}} = 14.838 \text{ nS/pF}$
maximal I_{CaL} conductance	$G_{\text{CaL}} = 3.98 \cdot 10^{-5} \text{ cm}^3 \mu\text{F}^{-1} \text{s}^{-1}$
maximal I_{Ks} conductance	$G_{\text{Ks}} = 0.098 \text{ nS/pF}$
maximal I_{to} conductance	$G_{\text{to}} = 0.294 \text{ nS/pF}$
maximal I_{Kr} conductance	$G_{\text{Kr}} = 0.153 \text{ nS/pF}$
maximal I_{K1} conductance	$G_{\text{K1}} = 5.405 \text{ nS/pF}$
maximal I_{pK} conductance	$G_{\text{pK}} = 0.0146 \text{ nS/pF}$
maximal I_{bNa} conductance	$G_{\text{bNa}} = 0.00029 \text{ nS/pF}$
maximal I_{bCa} conductance	$G_{\text{bCa}} = 0.000592 \text{ nS/pF}$
maximal I_{pCa} conductance	$G_{\text{pCa}} = 0.1238 \text{ nS/pF}$
maximal I_{SAC} conductance	$G_{\text{SAC}} = 0.0375 \text{ mS/cm}^2$
maximal I_{NaCa}	$k_{\text{NaCa}} = 1.0 \text{ pA/pF}$
voltage dependenced parameter of I_{NaCa}	$\gamma = 0.35$
factor enhancing outward nature of I_{NaCa}	$\alpha = 2.5$
saturation factor for I_{NaCa}	$k_{\text{sat}} = 0.1$
Na half-saturation constant for I_{NaCa}	$\text{K}_{\text{mNa}_i} = 87.5 \text{ mM}$
Ca half-saturation constant for I_{NaCa}	$\text{K}_{\text{mCa}} = 1.38 \text{ mM}$
K_e half-saturation constant for I_{NaK}	$\text{K}_{\text{mK}} = 1 \text{ mM}$
Na half-saturation constant for I_{NaK}	$\text{K}_{\text{mNa}} = 40 \text{ mM}$
Ca half-saturation constant of I_{pCa}	$\text{K}_{\text{pCa}} = 0.0005 \text{ mM}$
relative I_{Ks} permeability to Na^+	$p_{\text{KNa}} = 0.03$
SAC reversal potential	$E_{\text{SAC}} = -20 \text{ mV}$
SAC equilibrium constant	$\kappa_e = 100$
stretch sensitivity of I_{SAC}	$\alpha_{\text{SAC}} = 3$
subspace volume	$V_{\text{SS}} = 5.468 \cdot 10^{-5} \text{ mm}^3$
sarcoplasmic reticulum volume	$V_{\text{SR}} = 0.001094 \text{ mm}^3$
maximal I_{leak} conductance	$V_{\text{leak}} = 0.00036 \text{ mM/ms}$
maximal I_{up} conductance	$V_{\text{maxup}} = 0.006375 \text{ mM/ms}$
half saturation constant of I_{up}	$K_{\text{up}} = 0.00025 \text{ mM}$
maximal I_{rel} conductance	$V_{\text{rel}} = 0.102 \text{ mM/ms}$
maximal I_{xfer} conductance	$V_{\text{xfer}} = 0.0038$
\bar{R} to \bar{O} and RI to I I_{rel} transition rate	$k_{1'} = 0.15$
\bar{O} to I and \bar{R} to RI I_{rel} transition rate	$k_{2'} = 0.045$
\bar{O} to \bar{R} and I to RI I_{rel} transition rate	$k_3 = 0.06$
I to \bar{O} and RI to I I_{rel} transition rate	$k_4 = 0.005 \text{ s}^{-1}$

TABLE 3. Parameters in the Courtemanche cell model.

gas constant	$R = 8314.472 \text{ mJK}^{-1}\text{mol}^{-1}$
temperature	$T = 310 \text{ K}$
Faraday constant	$F = 96485.3415 \text{ C/mol}$
valence of the ionic species	$z = 1 \text{ for Na and K, } z = 2 \text{ for Ca}$
intracellular volume	$V_i = 13668$
maximal I_{Na} conductance	$g_{\text{Na}} = 7.8 \text{ nS/pF}$
maximal I_{K1} conductance	$g_{\text{K1}} = 0.09 \text{ nS/pF}$
maximal I_{to} conductance	$g_{\text{to}} = 0.1652 \text{ nS/pF}$
maximal I_{Kr} conductance	$g_{\text{Kr}} = 0.029411765 \text{ nS/pF}$
maximal I_{Ks} conductance	$g_{\text{Ks}} = 0.12941176 \text{ nS/pF}$
maximal $I_{\text{Ca,L}}$ conductance	$g_{\text{Ca,L}} = 0.12375 \text{ nS/pF}$
maximal $I_{\text{b,Ca}}$ conductance	$g_{\text{b,Ca}} = 0.001131 \text{ nS/pF}$
maximal $I_{\text{b,Na}}$ conductance	$g_{\text{b,Na}} = 0.000644375 \text{ nS/pF}$
maximal I_{NaK}	$I_{\text{NaK(max)}} = 0.59933874 \text{ pA/pF}$
maximal I_{NaCa}	$I_{\text{NaCa(max)}} = 1600$
maximal $I_{\text{p,Ca}}$	$I_{\text{pCa(max)}} = 0.275 \text{ pA/pF}$
maximal I_{up}	$I_{\text{up(max)}} = 0.005 \text{ mMms}^{-1}$
extracellular K^+ concentration	$\text{K}_e = 5.4 \text{ mM}$
extracellular Na^+ concentration	$\text{Na}_e = 140 \text{ mM}$
extracellular Ca^{2+} concentration	$\text{Ca}_e = 1.8 \text{ mM}$
Na^+ half saturation constant for I_{NaK}	$K_{\text{m,Na}} = 10 \text{ mM}$
Na_e^+ half saturation constant for I_{NaCa}	$K_{\text{m,Na(e)}} = 87.5 \text{ mM}$
Ca_e^{2+} half-saturation constant for I_{NaCa}	$K_{\text{m,Ca}} = 1.38$
K_e^+ half saturation constant for I_{NaK}	$K_{\text{m,K(e)}} = 1.5 \text{ mM}$
saturation factor for I_{NaCa}	$k_{\text{sat}} = 0.1$
voltage dependence parameter for I_{NaCa}	$\gamma = 0.35$
Ca^{2+} half-saturation constant for I_{up}	$k_{\text{up}} = 0.00092 \text{ mM}$
maximal release rate for I_{rel}	$k_{\text{rel}} = 30 \text{ ms}^{-1}$
total troponin concentration in myoplasm	$\text{Trpn}_{\text{max}} = 0.07 \text{ mM}$
total calmodulin concentration in myoplasm	$\text{Cmdn}_{\text{max}} = 0.05 \text{ mM}$
total calsequestrin concentration in SR release compartement	$\text{Csqn}_{\text{max}} = 10 \text{ mM}$
Ca half-saturation constant for troponin	$K_{\text{m,Trpn}} = 0.0005 \text{ mM}$
Ca half-saturation constant for calmodulin	$K_{\text{m,Cmdn}} = 0.00238 \text{ mM}$
Ca_{rel} half-saturation constant for I_{up}	$K_{\text{m,Csqn}} = 0.8 \text{ mM}$
temperatur scaling factor for $I_{\text{K ur}}$ and I_{to}	$K_{\text{Q10}} = 3$
maximal Ca^{2+} concentration in NSR	$\text{Ca}_{\text{up,max}} = 15 \text{ mM}$
V_{CaL}	65 mV
V_{Kr1}	15 mV
V_{Kr2}	22.4 mV
V_{K1}	80 mV

APPENDIX B. HYPERELASTIC PARAMETERS

In this section we present all parameters used in the mechanical models of the previous chapters. First, the initial values of all parameters used in the Land force model are given in Tab. 4.

TABLE 4. Parameters in the Land cell model.

Unbinding rate	$k_{\text{Tr}} = 0.1 \text{ ms}^{-1}$
Cooperativity of calcium-troponin binding rate	$n_{\text{Tr}} = 2$
Half-activation point concentration	$\text{Ca}_{\text{T50}}^{\text{ref}} = 0.805 \text{ } \mu\text{M}$
	$k_B = 0.1 \text{ ms}^{-1}$
Cooperativity of troponin and unblocked binding sites	$n_{\text{Tr}B} = 5$
	$k_{\text{UW}} = 0.182 \text{ ms}^{-1}$
	$k_{\text{WS}} = 0.012 \text{ ms}^{-1}$
Steady-state ration for state W	$r_W = 0.50$
Steady-state ration for state S	$r_S = 0.25$
	$\gamma_W = 0.615$
	$\gamma_S = 0.0085$
proportionality of steady-state crossbridge cycling rates	$\phi = 2.23$
Instantaneous distortion magnitude	$A_{\text{eff}} = 25$
	$\beta_0 = 2.3$
	$\beta_1 = -2.4$
Maximal active tension at resting length	$T_{\text{ref}} = 120 \text{ kPa}$

Next, the fitted parameters for the force-length-relationship $R_{\text{F-L}}$ are presented in Tab. 5.

TABLE 5. Parameters of the force-length relationship function

Sarcomere lengths	$l_{\min} = 0.00170 \text{ mm}$	$l_{\max} = 0.00260 \text{ mm}$
	$l_0 = 0.00195 \text{ mm}$	
Fourier coefficients	$c_0 = -4333.618335582119$	$d_0 = -2051.827278991976$
	$c_1 = 2570.395355352195$	$d_1 = 302.216784558222$
	$c_2 = 1329.536116891330$	$d_2 = 218.375174229422$
	$c_3 = 104.943770305116$	

The values for the different passive material models are given in Tab. 6.

TABLE 6. Parameters of the passive material models

Guccione Model	$C_0 = 876 \text{ Pa}$	$b_1 = 18.48$
		$b_2 = 3.58$
		$b_3 = 1.627$
Holzappel-Ogden Model	$a = 59 \text{ Pa}$	$b = 8.023$
	$a_{\text{f}} = 18472 \text{ Pa}$	$b_{\text{f}} = 16.026$
	$a_{\text{s}} = 2481 \text{ Pa}$	$b_{\text{s}} = 11.120$
	$a_{\text{fs}} = 216 \text{ Pa}$	$b_{\text{fs}} = 11.436$
Volumetric Part Γ_λ	$\lambda = 2 \cdot 10^5 \text{ Pa}$	

APPENDIX C. CIRCULATORY SYSTEM PARAMETERS

In this section we present all parameters and initial values that are used for the circulatory system model introduced in the previous chapters. The parameters are given in Tab. 8, while the initial conditions are set to the values shown in Tab. 7.

TABLE 7. Initial conditions of the circulatory system model.

total volume	$V_{\text{tot}} = 5500 \text{ ml}$
systemic aortic volume	$V_{\text{SysArt}} = 969.453 \text{ ml}$
pulmonary arterial volume	$V_{\text{PulArt}} = 261.202 \text{ ml}$
pulmonary venous volume	$V_{\text{PulVen}} = 281.373 \text{ ml}$
left ventricular pressure	$p_{\text{Lv}} = 1066.578923 \text{ Pa}$
left atrial pressure	$p_{\text{La}} = 1066.578923 \text{ Pa}$
right ventricular pressure	$p_{\text{Rv}} = 533.289461 \text{ Pa}$
right atrial pressure	$p_{\text{Ra}} = 533.289461 \text{ Pa}$

TABLE 8. Parameters in the circulatory system model.

systemic aortic valve resistance	$R_{\text{SysArtValve}} = 0.799934 \text{ Pa}\cdot\text{s}\cdot\text{ml}^{-1}$
systemic aortic resistance	$R_{\text{SysArt}} = 9.332566 \text{ Pa}\cdot\text{s}\cdot\text{ml}^{-1}$
systemic aortic compliance	$C_{\text{SysArt}} = 0.015001234039 \text{ ml}\cdot\text{Pa}^{-1}$
systemic aortic unstressed Volume	$V_{\text{SysArtUnstr}} = 800 \text{ ml}$
systemic peripheral resistance	$R_{\text{SysPer}} = 119.990129 \text{ Pa}\cdot\text{s}\cdot\text{ml}^{-1}$
systemic venous resistance	$R_{\text{SysVen}} = 3.999671 \text{ Pa}\cdot\text{s}\cdot\text{ml}^{-1}$
systemic venous compliance	$C_{\text{SysVen}} = 0.750062 \text{ ml}\cdot\text{Pa}^{-1}$
systemic venous unstressed volume	$V_{\text{SysVenUnstr}} = 2850 \text{ ml}$
tricuspidal valve resistance	$R_{\text{RavValve}} = 0.399967 \text{ Pa}\cdot\text{s}\cdot\text{ml}^{-1}$
pulmonary arterial valve resistance	$R_{\text{PulArtValve}} = 0.399967 \text{ Pa}\cdot\text{s}\cdot\text{ml}^{-1}$
pulmonary arterial resistance	$R_{\text{PulArt}} = 2.666447 \text{ Pa}\cdot\text{s}\cdot\text{ml}^{-1}$
pulmonary arterial compliance	$C_{\text{PulArt}} = 0.075006 \text{ ml}\cdot\text{Pa}^{-1}$
pulmonary arterial unstressed volume	$V_{\text{PulArtUnstr}} = 150 \text{ ml}$
pulmonary peripheral resistance	$R_{\text{PulPer}} = 9.332566 \text{ Pa}\cdot\text{s}\cdot\text{ml}^{-1}$
pulmonary venous resistance	$R_{\text{PulVen}} = 3.999671 \text{ Pa}\cdot\text{s}\cdot\text{ml}^{-1}$
pulmonary venous compliance	$C_{\text{PulVen}} = 0.112509255293 \text{ ml}\cdot\text{Pa}^{-1}$
pulmonary venous unstressed volume	$V_{\text{PulVenUnstr}} = 200 \text{ ml}$
mitral valve resistance	$R_{\text{LavValve}} = 0.399967 \text{ Pa}\cdot\text{s}\cdot\text{ml}^{-1}$

ACKNOWLEDGMENTS

The authors gratefully acknowledge the support of the German Research Foundation (DFG) by CRC 1173, and by the BMBF project 05M2016.

REFERENCES

- [Ambrosi et al., 2011] Ambrosi, D., Arioli, G., Nobile, F., and Quarteroni, A. (2011). Electromechanical coupling in cardiac dynamics: the active strain approach. *SIAM Journal on Applied Mathematics*, 71(2):605–621.
- [Andreianov et al., 2015] Andreianov, B., Bendahmane, M., Quarteroni, A., and Ruiz-Baier, R. (2015). Solvability analysis and numerical approximation of linearized cardiac electromechanics. *Math. Models Methods Appl. Sci.*, 25(05):959–993.

- [Augustin et al., 2016] Augustin, C. M., Neic, A., Liebmann, M., Prassl, A. J., Niederer, S. A., Haase, G., and Plank, G. (2016). Anatomically accurate high resolution modeling of human whole heart electromechanics: a strongly scalable algebraic multigrid solver method for nonlinear deformation. *J. Computat. Phys.*, 305:622–646.
- [Barbarotta et al., 2018] Barbarotta, L., Rossi, S., Dedè, L., and Quarteroni, A. (2018). A transmurally heterogeneous orthotropic activation model for ventricular contraction and its numerical validation. *International journal for numerical methods in biomedical engineering*, 34(12):e3137.
- [Cherry et al., 2017] Cherry, E. M., Fenton, F. H., Krogh-Madsen, T., Luther, S., and Parlitiz, U. (2017). Introduction to focus issue: Complex cardiac dynamics.
- [Colli Franzone et al., 2017] Colli Franzone, P., Pavarino, L., and Scacchi, S. (2017). Effects of mechanical feedback on the stability of cardiac scroll waves: A bidomain electro-mechanical simulation study. *Chaos*, 27(9):093905.
- [Courtemanche et al., 1998] Courtemanche, Marc, Ramirez, J. R., Nattel, and Stanley (1998). Ionic mechanisms underlying human atrial action potential properties: insights from a mathematical model. *American Journal of Physiology-Heart and Circulatory Physiology*, 275(1):H301–H321.
- [Crisfield, 1997] Crisfield, M. A. (1997). *Non-linear Finite Element Analysis of Solids and Structures*, volume 2. Wiley.
- [Cronin and Jane, 1987] Cronin and Jane (1987). *Mathematical aspects of Hodgkin-Huxley neural theory*, volume 7. Cambridge University Press.
- [Fedele et al., 2017] Fedele, M., Faggiano, E., Dede, L., and Quarteroni, A. (2017). A patient-specific aortic valve model based on moving resistive immersed implicit surfaces. *Biomechanics and Modeling in Mechanobiology*, 16(5):1779–1803.
- [Franzone et al., 2014] Franzone, P. C., Pavarino, L. F., and Scacchi, S. (2014). *Mathematical cardiac electrophysiology*, volume 13. Springer.
- [Franzone et al., 2015] Franzone, P. C., Pavarino, L. F., and Scacchi, S. (2015). Parallel multilevel solvers for the cardiac electro-mechanical coupling. *Appl. Numer. Math.*, 95:140–153.
- [Guccione et al., 1991] Guccione, J. M., McCulloch, A. D., and Waldman, L. K. (1991). Passive material properties of intact ventricular myocardium determined from a cylindrical model. *Journal of Biomechanical Engineering*, 113:42–55.
- [Holzapfel and Ogden, 2009] Holzapfel, G. A. and Ogden, R. W. (2009). Constitutive modelling of passive myocardium: a structurally based framework for material properties. *Philosophical Transactions of the Royal Society A*, 367:3445–3475.
- [Kohl et al., 2001] Kohl, Peter, Sachs, and Frederick (2001). Mechanoelectric feedback in cardiac cells. *Philosophical Transactions of the Royal Society of London. Series A: Mathematical and Physical and Engineering Sciences*, 359(1783):1173–1185.
- [Land et al., 2015] Land, S., Gurev, V., Arens, S., Augustin, C. M., Baron, L., Blake, R., Bradley, C., Castro, S., Crozier, A., Favino, M., Fastl, T. E., Fritz, T., Gao, H., Gizzi, A., Griffith, B. E., Hurtado, D. E., Krause, R., Luo, X., Nash, M. P., Pezzuto, S., Plank, G., Rossi, S., Ruprecht, D., Seemann, G., Smith, N. P., Sundnes, J., Rice, J. J., Trayanova, N., Wang, D., Wang, Z. J., and Niederer, S. A. (2015). Verification of cardiac mechanics software: benchmark problems and solutions for testing active and passive material behaviour. *Proceedings of the Royal Society A: Mathematical, Physical and Engineering Sciences*, 471(2184).
- [Land et al., 2017] Land, S., Park-Holohan, S.-J., Smith, N. P., dos Remedios, C. G., Kentish, J. C., and Niederer, S. A. (2017). A model of cardiac contraction based on novel measurements of tension development in human cardiomyocytes. *Journal of Molecular and Cellular Cardiology*, 106:68–83.
- [Niederer et al., 2011] Niederer, S. A., Kerfoot, E., Benson, A. P., Bernabeu, M. O., Bernus, O., Bradley, C., Cherry, E. M., Clayton, R., Fenton, F. H., Garny, A., et al. (2011). Verification of cardiac tissue electrophysiology simulators using an N-version benchmark. *Phil. Trans. R. Soc. A*, 369(1954):4331–4351.
- [Pathmanathan et al., 2013] Pathmanathan, P., Ortner, C., and Kay, D. (2013). Existence of solutions of partially degenerate visco-elastic problems, and applications to modelling muscular contraction and cardiac electro-mechanical activity.
- [Pavarino et al., 2017] Pavarino, L., Scacchi, S., Verdi, C., Zampieri, E., and Zampini, S. (2017). Scalable BDDC algorithms for cardiac electromechanical coupling. In *Domain Decomposition Methods in Science and Engineering XXIII*, pages 261–268. Springer.
- [Quarteroni et al., 2017] Quarteroni, A., Lassila, T., Rossi, S., and Ruiz-Baier, R. (2017). Integrated heart-coupling multiscale and multiphysics models for the simulation of the cardiac function. *Comput. Methods Appl. Mech. Eng.*, 314:345–407.
- [Quarteroni et al., 2019] Quarteroni, A., Manzoni, A., Vergara, C., et al. (2019). *Mathematical modelling of the human cardiovascular system: data, numerical approximation, clinical applications*, volume 33. Cambridge University Press.
- [Rossi et al., 2012] Rossi, S., Ruiz-Baier, R., Pavarino, L. F., and Quarteroni, A. (2012). Orthotropic active strain models for the numerical simulation of cardiac biomechanics. *International Journal for Numerical Methods in Biomedical Engineering*, 28:761–788.
- [Ruiz-Baier et al., 2014] Ruiz-Baier, R., Gizzi, A., Rossi, S., Laadhari, A., Filippi, S., and Quarteroni, A. (2014). Mathematical modelling of active contraction in isolated cardiomyocytes. *Mathematical Medicine and Biology*, 31:259–283.
- [Santiago et al., 2018] Santiago, A., Zavala-Aké, M., Aguado-Sierra, J., Doste, R., Gómez, S., Arís, R., Cajas, J. C., Casoni, E., and Vázquez, M. (2018). Fully coupled fluid-electro-mechanical model of the human heart for supercomputers. *Int. J. Numer. Methods Biomed. Eng.* online first.
- [Tagliabue et al., 2017] Tagliabue, A., Dedè, L., and Quarteroni, A. (2017). Complex blood flow patterns in an idealized left ventricle: A numerical study. *Chaos: An Interdisciplinary Journal of Nonlinear Science*, 27(9):093939.

- [Tavi et al., 1998] Tavi, Pasi, Han, Chunlei, Weckström, and Matti (1998). Mechanisms of stretch-induced changes in $[Ca^{2+}]_i$ in rat atrial myocytes: role of increased troponin c affinity and stretch-activated ion channels. *Circulation research*, 83(11):1165–1177.
- [ten Tusscher and Panfilov, 2006] ten Tusscher, K. H. and Panfilov, A. V. (2006). Alternans and spiral breakup in a human ventricular tissue model. *American Journal of Physiology-Heart and Circulatory Physiology*.